Effects of Transcranial Magnetic Stimulation Informed by Electrophysiological Biomarkers in Non-Human Primates and Humans

A DISSERTATION SUBMITTED TO THE FACULTY OF
UNIVERSITY OF MINNESOTA
BY

Nipun Dilesh Perera

IN PARTIAL FULFILLMENT OF THE REQUIREMENTS
FOR THE DEGREE OF
DOCTOR OF PHILOSOPHY

Advisor: Alexander Opitz

October 2024

Acknowledgements

First and foremost, I would like to thank Prof. Alexander Opitz for accepting me under his wing as a PhD student and for his continued support and mentorship throughout my PhD. I’m grateful for the opportunities he gave me to explore the field of non-invasive brain stimulation and the guidance he provided to gain invaluable skills. I owe it to his valuable and honest insights that enabled me to realize my strengths and weaknesses and become a well-rounded researcher.

I appreciate my committee members Prof. Theoden Netoff, Prof. Matthew D Johnson, Prof. Luke Johnson and Prof. Jan Zimmermann whose valuable feedback and advice shaped the projects I worked on and kept me on the right track.

My sincere gratitude goes to our collaborators, Dr. Arnaud Falchier, Dr. Brian E. Russ, Dr. Gary Linn, Brent Butler and Kurt Masiello who were instrumental in running the non-human primate experimental work.

I would like to thank immensely my lab members, especially Dr. Sina Shirinpour who, from the beginning of my PhD, almost to the end, tolerated all my questions and annoyances and was a supportive office mate. Furthermore, I appreciate the guidance I received from Dr. Miles Wischnewski, Dr. Ivan Alekseichuk and Dr. Kathleen Mantell throughout my PhD career. I also thank the rest of the current lab members including Dr. Harry Tran, Taylor Berger, Zhihe Zhao, Zach Haigh, Dr.

Sangjun Lee, Dr. Malte Güth, Da Som Choi and Zijia Jin for being supportive lab mates.

Additionally, I thank the faculty and staff of the BME department for their academic and administrative support. I specifically want to thank Prof. Alena Talkachova, Prof. Casim Sarkar and Prof. David Wood, Prof. Brenda Ogle, Rachel Jorgenson and Sarah Erickson for always looking out for graduate students.

Also, my sincere gratitude extends to the tax paying general public in Sri Lanka and the United States of America, whose work funded my education for 23 years. Similarly, I would like to thank the National Institutes of Health (NIH) and MnDRIVE for their financial support during my PhD program.

I am immensely thankful to everyone in my personal life including my friends from Sri Lanka, the friends I made in Minnesota who have uplifted me intellectually and emotionally throughout my life. Furthermore, I am sincerely grateful to Ashley Groebner who has been there for me for the last year of my PhD, for being a cheerful supporter. Finally, I am wholeheartedly grateful to silent heroes of my life, that is, my family including my parents and my sister for supporting my endeavors throughout my life and having faith in the choices I made.

"A man travels the world over in search of what he needs, and returns home to find it." — George A. Moore

Abstract

Transcranial Magnetic Stimulation (TMS) is a non-invasive brain stimulation technique that leverages time-varying magnetic fields to induce electric fields that modulate brain activity. It is used in research to study causal brain effects and in clinical settings as a therapeutic tool for neuropsychiatric disorders. Despite the clinical utility, its mechanisms of action are not fully understood. Specifically, the effects of TMS dose, stimulation location and the ambiguity of centrally and peripherally induced effects have not been extensively studied. The standard approach for studying these mechanisms is TMS-EEG in humans which has constraints due to limited spatial specificity. Non-human primate (NHP) models, when combined with invasive electrophysiology, present the unique opportunity of studying these mechanisms with a high spatial specificity. In my first study, I investigated electrophysiological biomarkers of TMS induced brain responses in NHPs with implanted stereotactic EEG electrodes (sEEG). Using these biomarkers, I quantified the dose and location dependent effects of TMS on NHP brain. Furthermore, with carefully designed control experiments, I dissociated centrally induced neural responses from peripherally induced auditory and somatosensory responses. Next, I extended this work to study the biomarkers relevant to TMS effects on human brain. I studied the brain mechanisms pertaining to state-dependent stimulation of human primary motor cortex (M1) using TMS-EEG. Specifically, I investigated the cortical brain responses evoked by stimulating

M1 at four phases of primary motor cortical oscillations, mu (8-13 Hz) and beta (14-30 Hz). I compared these responses with behavioral responses measured as motor evoked potentials (MEPs) to elucidate the phase dependent mechanisms of M1. I further studied the importance of oscillatory power on cortical response generation. Collectively, the results of these studies facilitate our understanding about TMS mechanisms. The NHP experiments are highly relevant for interpreting human TMS studies while human experiments are important for interpretation and development of biomarkers for TMS target engagement in clinical applications.

Contents

List of Tables

List of Figures

List of Abbreviations

ACC	Anterior Cingulate Cortex
AUD	Auditory Cortex
CC	Corpus Callosum
CN	Caudate Nucleus
CNS	Central Nervous System
DBS	Deep Brain Stimulation
DLPFC	Dorsolateral Prefrontal Cortex
dPCG	dorsal Posterior Cingulate Gyrus
ECoG	Electrocorticography
ECT	Electroconvulsive Therapy
EEG	Electroencephalography
EMG	Electromyography
ERP	Event Related Potential
ETP	Educated Temporal Prediction
FDA	Food and Drug Administration
FDI	First Dorsal Interosseus
FEF	Frontal Eye Field
fMRI	Functional Magnetic Resonance Imaging
FST	Fundus of Superior Temporal Visual Area
iEEG	Intracortical Electroencephalography
LFP	Local Field Potential
LIP	Lateral Intraparietal Area
M1	Primary Motor Cortex
MDD	Major Depressive Disorder
MEP	Motor Evoked Potential
MIP	Medial Intraparietal Area

MRI	Magnetic Resonance Imaging
MSO	Maximum Stimulator Output
MST	Medial Superior Temporal Area
MT	Middle Temporal Area
NHP	Non-Human Primates
OFC	Orbitofrontal Cortex
PCC	Posterior Cingulate Cortex
PEEK	Polyetheretherketone
PEST	Parameter Estimation by Sequential Testing
PFC	Prefrontal Cortex
PO	Preoptic Area
PPI	Phase Preservation Index
rmANOVA	Repeated-Measures Analysis of Variance
rMT	Resting Motor Threshold
S2	Secondary Somatosensory Cortex
SD/STD	Standard Deviation
SEM	Standard Error of Mean
STP	Superior Temporal Plane
TEM	Temporal Cortex
TEP	TMS-Evoked Potential
TMS	Transcranial Magnetic Stimulation
VX	Visual Area X (X = 1, 2, 3, 4)

Chapter 1: Introduction

1.1. Brain

The brain is akin to the central processing unit of a computer. Instead of billions of transistors, billions of neurons combine to form this fascinating organ that drives everything from the simplest to the most complex human behaviors. Neurons receive information from sensory cells or interneurons, integrate it, and transmit signals to effectors or other neurons through a series of electrical and chemical reactions. In the mammalian central nervous system (CNS), communication between neurons occurs at junctions known as synapses. Neurotransmitters released from the presynaptic neuron bind to receptors in the postsynaptic neuron. When a sufficient number of presynaptic inputs reach a neuron's dendrites, the membrane voltage reaches a threshold that triggers the neuron to produce an action potential (Lovinger, 2008). This action potential propagates along the axon and reaches the effector or another neuron through a series of depolarizations and ion influxes (Grider et al., 2024).

Neurons form groups that are functionally segregated and serve specific tasks (Tononi et al., 1994). These populations are organized into functional networks that govern complex human behavior and cognition. Over the years, researchers have been studying the mysteries of the brain at different levels of organization. Like any other organ, the brain's function can be disrupted by environmental and genetic factors, infections, injuries, and lifestyle choices, leading to pathological conditions. A subset of these pathologies includes neurological and psychiatric disorders, which are prevalent across all demographics. These disorders impose a heavy economic and societal burden in the U.S. and worldwide. In 2019, the economic burden for major depressive disorder (MDD) was estimated at $333.7 billion ($382.4 billion when adjusted for inflation in 2023), with 19.8 million individuals diagnosed (Greenberg et al., 2023). The COVID-19 pandemic of 2019-2021 exacerbated this mental health crisis (Brasso et al., 2023; Lewis et al., 2022; Young et al., 2023).

To treat neuropsychiatric disorders, several treatment methods have been introduced, such as psychotherapy, medication, and surgical interventions. In the 18th and 19th centuries, transcranial electrical stimulation (TES) methods, such as electroconvulsive therapy (ECT), were reported to generate feelings of euphoria and enhance mental performance (Kadosh & Elliott, 2013). More recently, invasive methods such as deep brain stimulation (DBS) have been introduced to treat these disorders. However, despite its promise in treating Parkinson's disease, DBS's utility is limited due to its invasive nature. In the quest for more effective, focal, and non-invasive treatments, Barker and colleagues introduced non-invasive magnetic stimulation of the human brain in 1985 (Barker et al., 1985; Horvath et al., 2011).

After almost 40 years since its introduction, transcranial magnetic stimulation (TMS) has made significant strides both as a research tool and as an FDA-approved therapeutic intervention for several neuropsychiatric disorders. In this dissertation, I will focus on TMS and its utility in research.

1.2. Recording Brain Electrophysiology

The activity of a single neuron is characterized by its spiking activity, which is measured via extracellular potentials using microelectrodes. In a neural population, the superposition of all ionic activities—including action potentials, synaptic activity, and ionic fluctuations from glial cells—results in an aggregate change in extracellular potential at a given time (Buzsáki et al., 2012). The temporal variation of this extracellular potential is known as the local field potential (LFP) and is measured using intracortical electroencephalography (iEEG) electrodes or electrocorticography (ECoG). While these recording modalities are invasive and therefore highly spatially specific, they cannot be readily used in humans. More commonly, electroencephalography (EEG) is used in research as a non-invasive recording modality. EEG measures a smoothed and attenuated version of the LFP and does not have a straightforward relationship with action potentials (Buzsáki et al., 2012).

Each modality has its own merits when recording brain activity. Single-unit and LFP recordings provide detailed insights into the underlying brain mechanisms with high spatial specificity, but their use is limited in human participants due to their invasive nature. EEG, on the other hand, is a readily available, low-cost tool that can be used non-invasively, albeit with a trade-off in spatial resolution. Regardless of the modality, recording brain activity allows us to explore the brain's electrophysiology, identify biomarkers related to physiological mechanisms, and investigate how these biomarkers are modulated in neurological and psychiatric disorders. These electrophysiological biomarkers provide objective measurements of brain activity and pathophysiology, making them valuable candidates for evaluating treatment efficacy and outcomes.

1.3. Transcranial Magnetic Stimulation (TMS)

Non-invasive brain stimulation has garnered attention over the last couple of decades for both its research and clinical utility (Peterchev et al., 2012). Transcranial magnetic stimulation (TMS) is arguably the most popular non-invasive method in the current neuromodulation landscape. TMS generates a transient, time-varying magnetic field by passing a pulse of current through a coil (Barker et al., 1985). When the coil is placed on the head, according to Faraday's law, the time-varying magnetic field induces an electric field in the brain. This electric field modulates the electric current profile of neurons (either excitation or inhibition), resulting in neural stimulation (Hallett, 2007). An example of the electric field distribution resulting from TMS stimulation is shown in Figure 1.1.

The effects and utility of TMS vary depending on the location of stimulation. For example, delivering single-pulse TMS to the motor cortex elicits motor-evoked potentials (MEPs), which can be recorded using electromyography (EMG). This can serve as a direct measure of brain excitability, making TMS a valuable probing tool (Rothwell et al., 1999). Clinical applications of single-pulse TMS include assessing the integrity of motor pathways, particularly following conditions such as stroke, motor neuron disease, and multiple sclerosis. (Groppa et al., 2012; Sandbrink, 2008).

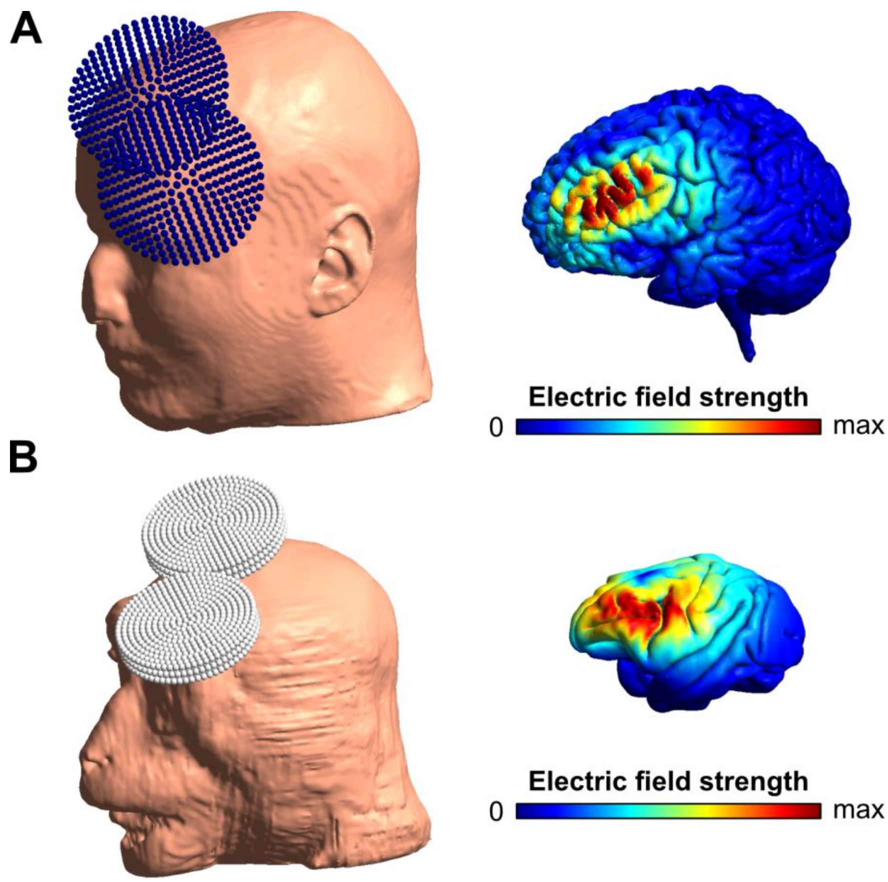

Figure 1.1 Transcranial Magnetic Stimulation (TMS). A) TMS coil placed on the prefrontal cortex of a human (left) and the magnitude of the induced electric field on the cortex (right). B) TMS coil placed on the prefrontal cortex of a non-human primate (left) with the magnitude of the induced electric field on the cortex (right).

On the other hand, repetitive application of TMS, known as repetitive TMS (rTMS), to the prefrontal brain regions has been used for the clinical treatment of psychiatric disorders. In rTMS, a train of single pulses is applied rhythmically with a specific frequency and temporal profile (Ziemann, 2017). Depending on the rTMS protocol used, long-term depression (LTD) or long-term potentiation (LTP)-like synaptic plasticity can be induced in the brain (Gersner et al., 2011; Jannati et al., 2023). Application of rTMS to the dorsolateral prefrontal cortex (DLPFC) has been shown to be effective in alleviating symptoms of major depressive disorder (MDD), obsessive-compulsive disorder (OCD), attention deficit hyperactivity disorder (ADHD), and in smoking cessation (Brunoni et al., 2017; Lusicic et al., 2018; T. Perera et al., 2016; Zangen et al., 2021) and has been FDA-approved for use in these disorders.

Despite its importance and prevalence as a therapeutic tool, there are still major gaps in our understanding of the mechanisms of action of TMS. Specifically, the dose-dependent effects of TMS and how biomarkers of TMS activity vary with dose have not been extensively studied. Furthermore, knowledge about the extent of the area stimulated by TMS and the coil-location-dependent behavior of biomarkers is sparse in the current literature. Another source of ambiguity in TMS stimulation is peripheral auditory and somatosensory stimulation, which can confound the central nervous system-mediated response (Conde et al., 2019).

The standard approach to studying these issues is concurrent TMS-EEG in humans. However, the limited spatial specificity inherent to this method prevents us from accurately delineating the biomarkers of TMS activation and separating peripheral responses from central brain responses. To overcome this limitation, invasive electrophysiology, which provides superior spatial resolution, can be used. However, due to ethical concerns, this cannot be readily performed in humans. Non-human primates offer a unique opportunity to study these issues using invasive recording techniques. Therefore, one of the projects presented in this dissertation focuses on addressing these knowledge gaps using invasive electrophysiology in non-human primates.

In recent years, the use of real-time, closed-loop, state-dependent TMS stimulation has gained attention due to its potential to improve treatment efficacy in therapeutic applications. Most closed-loop systems target the phase of brain oscillations, which is indicative of the current brain state. Existing studies have examined the modulation of behavioral outcomes (e.g., motor-evoked potentials when targeting the motor cortex) during phase-dependent stimulation. However, the effects of such stimulation on electrophysiological biomarkers and their relationship with behavioral measures have not been studied in depth in humans. Understanding the effects of state-dependent stimulation will enable us to quantify treatment outcomes and develop objective measures of brain function. Therefore, the second project in this dissertation focuses on studying brain responses and their relationship to behavioral outcomes during phase-dependent stimulation of the human motor cortex.

1.4. Summary of Studies

In this dissertation, I address some of the aforementioned gaps in our understanding of TMS stimulation.

In Chapter 2, I detail the effects of single-pulse TMS on the non-human primate brain, recorded using invasive electrophysiology. I present how dose affects brain responses, quantified through electrophysiological biomarkers in local field potentials. Then, I use these biomarkers, along with electric field modeling, to study the effects of stimulation location on brain responses. Finally, I demonstrate how these biomarkers can be used to dissociate peripheral effects of TMS (i.e., auditory and somatosensory) from central effects.

In Chapter 3, I discuss the effects of real-time, phase-dependent stimulation on EEG biomarkers in the human motor cortex. I also investigate the relationship between these biomarkers and previously analyzed MEP data to explain the origins of cortical responses and corticospinal excitability. Finally, I examine the role of pre-TMS oscillatory power in brain responses, as well as the role of sensorimotor mu and beta oscillations in modulating brain responses in the motor cortex.

In Chapter 4, I draw conclusions from these two studies and discuss the implications of the findings. I further elaborate on how these findings are relevant to current research and potential future directions, particularly in clinical applications.

Chapter 2: Effects of TMS in Non-human Primates

2.1. Introduction

Modulating local neural activity has great potential to restore affected brain regions in neurologic and psychiatric disorders. Non-invasive neuromodulation is a cost-effective tool for largescale use in patients with a wide range of symptoms and symptom severity. The current gold standard for non-invasive neuromodulation in clinical and basic research is transcranial magnetic stimulation (TMS). TMS can induce action potentials in neurons and, through its repeated application, brain plasticity (Hoogendam et al., 2010; Huang et al., 2005). TMS-based therapies received Food and Drug Administration approval to treat major depressive disorder, obsessive-compulsive disorder, and nicotine addiction (Brunoni et al., 2017; Lefaucheur et al., 2020). Despite its increasing use in research and clinical applications, the physiological effects of TMS are not fully understood. This gap of knowledge has hampered rational dose selection and optimization of TMS parameters. In particular, a clear physiological marker of TMS target engagement would be crucial to advance clinical applications in brain regions other than the motor cortex, such as the dorsolateral prefrontal cortex (DLPFC). In human research, TMS physiological effects can be measured non-invasively through motor-evoked potentials (MEPs; Brasil-Neto et al., 1992; Numssen et al., 2021;

Wischnewski et al., 2022), functional magnetic resonance imaging (fMRI; Denslow et al., 2005; Nahas et al., 2001; Oathes et al., 2021), and electroencephalography (EEG; Bonato et al., 2006; Daskalakis et al., 2008; Ilmoniemi et al., 1997; Massimini et al., 2005; Rogasch et al., 2015; Thut et al., 2011). Combined TMS-EEG is a promising method to study neural population responses to TMS with high temporal accuracy. A primary way of investigating transient stimulation effects on EEG is by measuring TMS-evoked potentials (TEPs). For example, causal brain dynamics during TMS perturbation in motor, visual, and prefrontal brain regions (Bonato et al., 2006; Ilmoniemi et al., 1997) and modulation of brain state during behavior (Massimini et al., 2005; Thut et al., 2011) have been studied through TMS-EEG. It has also been used to quantify cortical inhibition paradigms that are resulting from TMS perturbation (Daskalakis et al., 2008; Rogasch et al., 2015). However, despite its promise for studying the neural responses of TMS, the interpretation of human TMS-EEG neurophysiological results is challenging. One challenge for the interpretation of TMS-EEG is a poor spatial localization of results because of volume conduction, meaning that the location of TEP sources is unclear. Second, multisensory side effects during TMS include auditory and somatosensory coactivation (by TMS click sound and muscle and peripheral nerve co-stimulation), which also affect brain responses. This results in a challenge to disentangle stimulation effects induced in the brain because of the TMS electric field and peripheral sensory stimulation effects (Conde et al., 2019; Ilmoniemi & Kičić, 2010). For consistency, we define the following: (1) centrally induced TMS effects as the effects originating in the CNS [for a given brain area, such effects can be because of the (i) local electric field inducing suprathreshold depolarization of neurons or (ii) circuit-mediated activation propagated from another brain area where the TMS electric fields induced suprathreshold depolarization]; and (2) peripherally induced stimulation effects originate in the peripheral nervous system in the form of auditory or somatosensory activation and later propagate to the CNS. To systematically investigate TMS physiological mechanisms, several control conditions carefully accounting for various confounds are required (Biabani et al., 2019; Rocchi et al., 2021). Non-human primate (NHP) models can overcome the main limitations of human TMS-EEG. Using invasive electrophysiological recordings in NHPs offers a unique opportunity to study the physiological effects of TMS with high spatiotemporal precision and control for somatosensory effects. Further, compared with smaller animal models, the size and cortical folding patterns of the NHP brain will result in comparable TMS-induced electric fields as in the human brain, making them an ideal translational model (Alekseichuk et al., 2019). Previous work using TMS in NHPs has studied the effect of single-pulse TMS on single-unit activity (Mueller et al., 2014; Romero et al., 2019). These findings have shown that TMS (compared with sham stimulation) causes neural activity within milliseconds, and this effect is observed in various neuron types (Mueller et al., 2014). Furthermore, these effects are specific to the targeted area and affect behavioral responses (Romero et al., 2019). While these studies have resulted in important insights into TMS mechanisms, they were limited to the microscale neurophysiological level and a single brain location. However, it is well understood that TMS effects are widespread, involving several brain networks (Fox et al., 2012; Ozdemir et al., 2020). Furthermore, it is not straightforward to translate the findings from cellular response to EEG. On the other hand, invasive stereo-EEG recordings can measure mesoscale, neurocircuit activity across the brain while preserving excellent spatiotemporal precision. In addition, one can directly translate findings in local field potentials (LFPs) to the macroscale of human EEG. Here, we record TMS-evoked responses in the NHP brains with implanted depth electrodes along a whole hemisphere. Our experimental setup allows for answering previously unanswered key questions of TMS dose response and spatial specificity. First, we study the effects of TMS intensity and coil location on TEPs. Second, we measure TMS multisensory coactivation (both auditory and somatosensory effects) through exhaustive control experiments. Our results demonstrate clear TMS-evoked brain responses, that are separable from peripheral effects, with increasing doses corresponding to larger evoked responses. Additionally, we show spatial specificity of these physiological responses. Our findings are crucial for the interpretation of human TMS-EEG studies, rational dose control, and the development of robust markers of target engagement based on TMS-evoked potentials.

2.2. Materials and Methods

2.2.1. Non-human Primate Preparation

The NHP experiments were done at the Nathan Kline Institute (Orangeburg, NY). All procedures were approved by the Animal Care and Use Committee of the Nathan Kline Institute. We used two adult non-human primates (Macaca mulatta) in this study (Monkey W – female, 5 kg; Monkey H – male, 10 kg). The monkeys were implanted with an MRI compatible PEEK headpost positioned over the occipito-parietal region. Three multi-contact stereo electroencephalography (sEEG) depth electrodes (Ad-tech®, 5 mm spacing) were permanently implanted through a skull incision over the left occipital cortex. Recording electrodes were oriented along the posterior-anterior axis with medial prefrontal cortex, frontal eye field (FEF), auditory (AUD), and temporal cortex (TEM) as the endpoints. In monkey W, an additional electrode targeted the geniculate complex of the thalamus.

For both monkeys, we acquired the T1 and T2 spin echo (SE) sequences using a Siemens® TrioTim 3T scanner with the following parameters: pixel dimensions = 0.5 x 0.5 x 0.5 mm, flip angle = 80°, TR = 2600 ms, TE = 3.55 ms, and TI = 900 ms. Exact electrode positions were identified on a post-implantation MR image, registered to the pre-implantation image, and referenced to the common stereotaxic atlas (Saleem & Logothetis, 2012). See Table 2.1 and 2.2 for details. MRI registration was done using FSL's FLIRT package (Greve & Fischl, 2009;

Jenkinson et al., 2002; Jenkinson & Smith, 2001). The electrode positions with respect to the brain are shown in Figure 2.1a.

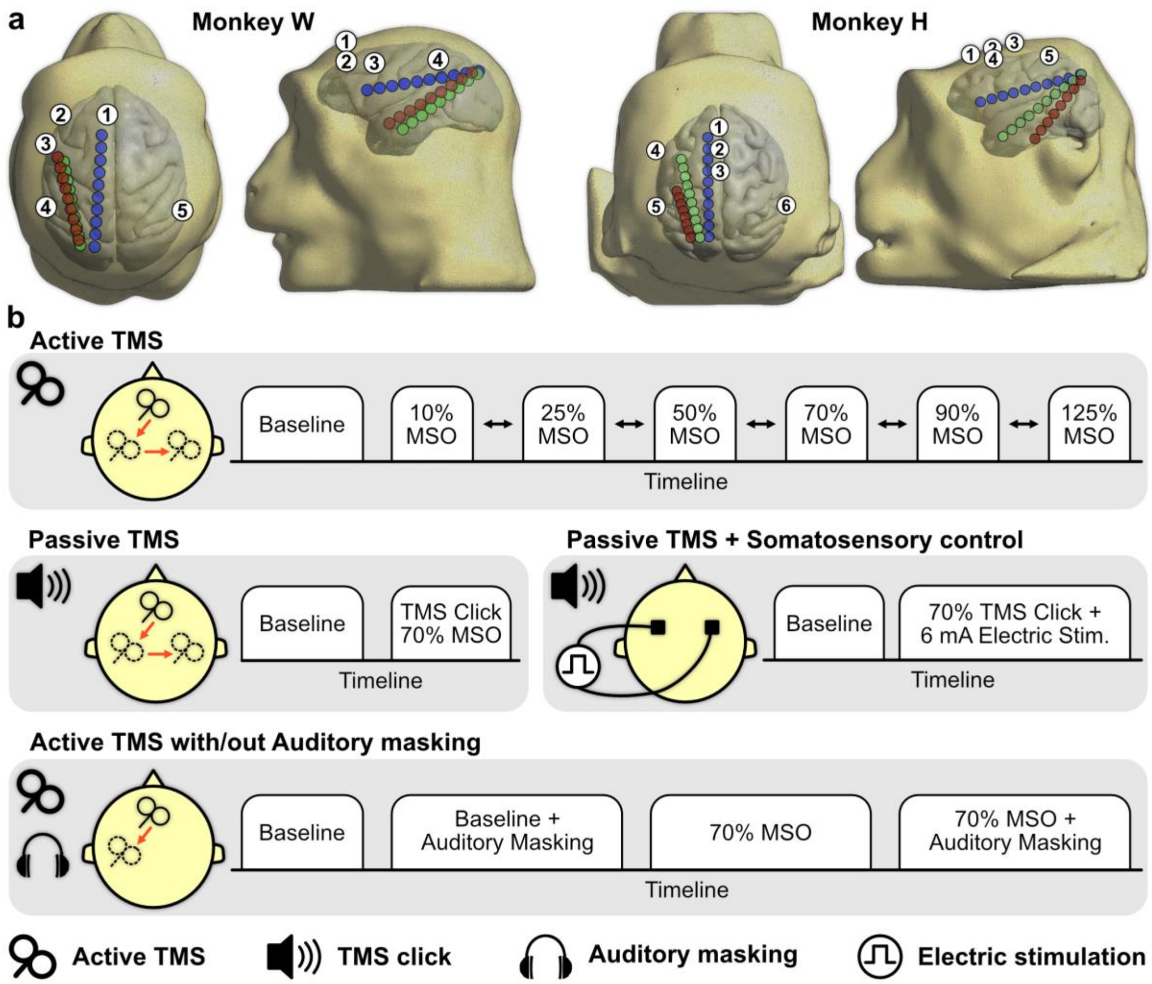

Figure 2.1 Overview of electrode implantation and experimental setup. a) Contact locations of invasive depth electrodes and TMS coil locations in the reconstructed head and brain surfaces of each monkey. The electrode shafts are directed at frontal eye fields (blue) and auditory (green) and temporal (red; superior temporal in Monkey W and inferior temporal in Monkey H) regions of the brain. TMS is delivered to five locations (numbered) in monkey W and 6 locations in Monkey H. b) Active TMS is delivered at 5 intensities (10, 25, 50, 70, and 90% of the maximum stimulator output, MSO) to both monkeys, with additional power mode setting of 125% MSO in Monkey H. For auditory control, TMS click is delivered at 70% MSO by turning the coil by 90 degrees away from the head, to mimic the auditory response. For somatosensory control, the scalp is stimulated with 6 mA electric pulse while delivering TMS click at 70% MSO. This control was performed at location 2 in monkey H. To control the effects of auditory co-activation, active TMS was delivered at 70% MSO with and without auditory masking at locations 1 and 5 in Monkey H.

Table 2.1 Monkey W – The anatomical regions associated with each contact of the sEEG electrodes

Contacts	FEF	AUD	TEM
1	CN (Head)	Auditory belt	TE
2	CN	Auditory belt/Insula	TE/STP
3	CN	Auditory belt/Insula	STP
4	CN	Auditory core/Insula	FST/STP
5	ACC/CC	S2	FST/STP
6	Dorsal bank of PCC (Area c)/CC	STP	MT
7	MIP	MT/STP	FST/TEO
8	MIP/LIP	V4	V4
9	PO/V3	V2	V2

Table 2.2 Monkey H – The anatomical regions associated with each contact of the sEEG electrodes.

Contacts	FEF	AUD	IT
1	CN/OFC	Ventral insular	Parahippocampal
2	CN	Ventral insular	FST
3	CN/CC	Temporal/Insular cortex	FST
4	CN/CC/AC	Insular cortex/Auditory lateral belt	FST/MT
5	CN/CC/AC	Auditory core/Insular cortex	MT
6	CC	Auditory core/S2	MT
7	CC	Auditory belt	WM
8	dPCG /MIP/LIP	Auditory belt/Brodmann's area 7A	WM
9	MIP	Brodmann's area 7A	MT
10	V1/V2	V3/V2	MT/MST

The brain morphology of the two monkeys were assessed by an expert in non-human primate anatomy. Monkey W has typical gross morphology with normal sulcal variability throughout the brain. Monkey H shows a variant of normal anatomy with multiple micro gyri in the parietal and occipital regions as well as enlarged ventricles in the posterior regions. The frontal, temporal, and deep brain areas are within the typical range of gross anatomy.

2.2.2. Transcranial Magnetic Stimulation (TMS)

We performed TMS experiments on the two non-human primate subjects in sphinx position. Monkeys were anesthetized with dexdomitor 0.015mg/kg IM, ketamine 6 mg/kg IM, atropine 0.045 mg/kg IM, followed by 1-2% isoflurane. In all experimental sessions, biphasic single-pulse TMS was delivered using a MagPro X100 (MagVenture®, Denmark) device with a butterfly coil MC-B35. The coil was positioned at locations designated in Figure 2.1a above the prefrontal cortex (Monkey W and H: position 1-2), premotor cortex (Monkey H: position 3), temporal areas (Monkey W: position 3, Monkey H: position 4), and auditory cortex (Monkey W: position 4, Monkey H: position 5). Stimulation location contralateral to the implanted sEEG electrodes, above the right temporal cortex (Monkey W: position 5, Monkey H: position 6) was used for both monkeys as a control condition. For frontal stimulation locations (Monkey W: position 1-3 and Monkey H: position 1-4), the coil orientation was maintained parallel to anterior-posterior line. Due to the intrusion of the head post on the lateral regions, for lateral stimulation locations (Monkey W: position 4-5 and Monkey H: position 5-6), the coil was oriented approximately 45^0 with respect to the anterior-posterior line. We ensured that the connectors and the wires to the electrodes were directed away from the coil and the stimulator, and the amplifier were substantially away from the monkey head during stimulation. For each location, we delivered five different TMS intensities in both NHPs: 10%, 25%, 50%, 70%, and 90% of maximum stimulator output (MSO). In addition, in Monkey H we applied 90% of maximum in power mode, equivalent to ~125% standard MSO. These intensities are linearly related to the current input (coil dI/dt) as follows: 10% MSO = 13 A/μs, 25% MSO = 37 A/μs, 50% MSO = 76 A/μs, 70% MSO = 107 A/μs, 90% MSO = 142 A/μs and 125% MSO = 201 A/μs. Each stimulation block (condition × location × intensity) consisted of ~80 TMS pulses given every 3–5 seconds.

We implemented the following experimental conditions (Figure 2.1b): I) Active TMS, II) Passive TMS (produces auditory click associated with TMS), III) Passive TMS with somatosensory control (adds focal electric pulse to the scalp), and IV) Active TMS with auditory masking (continuous auditory white noise masking auditory click associated with TMS).

In the passive TMS condition, we turned the TMS coil away from the head to solely mimic the TMS auditory response due to the click sound of the coil without direct brain stimulation. For auditory/somatosensory co-stimulation, we used MagVenture Cool-B65 A/P coil that concurrently provides electric current stimulation to the scalp. To study whether the current stimulation alone elicits peripheral effects, we used the sham coil in combination with the current stimulation over stimulation location 1. We delivered auditory click at 70% MSO along with 6 mA electrical stimulation on the scalp using pairs of 3M disc electrodes of 10mm diameter (3M®, Saint Paul, MN, USA) placed across the region of interest. This sham stimulation approach follows (Conde et al., 2019). Given that the cutaneous perception of electrical stimulation due to active TMS and somatosensory control cannot be assessed subjectively through feedback from non-human primates, we visually assessed and confirmed equivalent scalp and shoulder twitches during active and sham conditions.

For auditory masking, we created a masking acoustic noise using the TMS Adaptable Auditory Control tool (Russo et al., 2022). The sound pressure level of the masking noise was set to 80 dB for the above stimulation intensities. Sound pressure level was measured at the ear canal using a sound meter (Bruel and Kjaer®, Nærum, Denmark). The masking noise was presented via two speakers placed 50 mm from the head on each side. The masking was applied concurrently with active TMS at stimulation locations 1 and 5 with the intensity of 70% MSO.

2.2.3. Data Preprocessing and Electric Field Modeling

We recorded the local field potentials (LFPs) using 32-channel ActiveTwo amplifier (Cortech®, Wilmington, NC, USA) at a sampling rate of 40 kHz. For both monkeys, contacts in the occipital cortex (proximal to the headpost) were chosen as the reference and the ground (9th and 11th contacts from the front in the FEF electrode respectively). To prevent the electric current induction in the electrode contacts due to the magnetic field, we made sure that the recording setup, including the electrode contacts and the electrical cables, were free of loops. Furthermore, high input resistance of the amplifier (1 GΩ) would minimize induced currents to negligible levels, even if they occur.

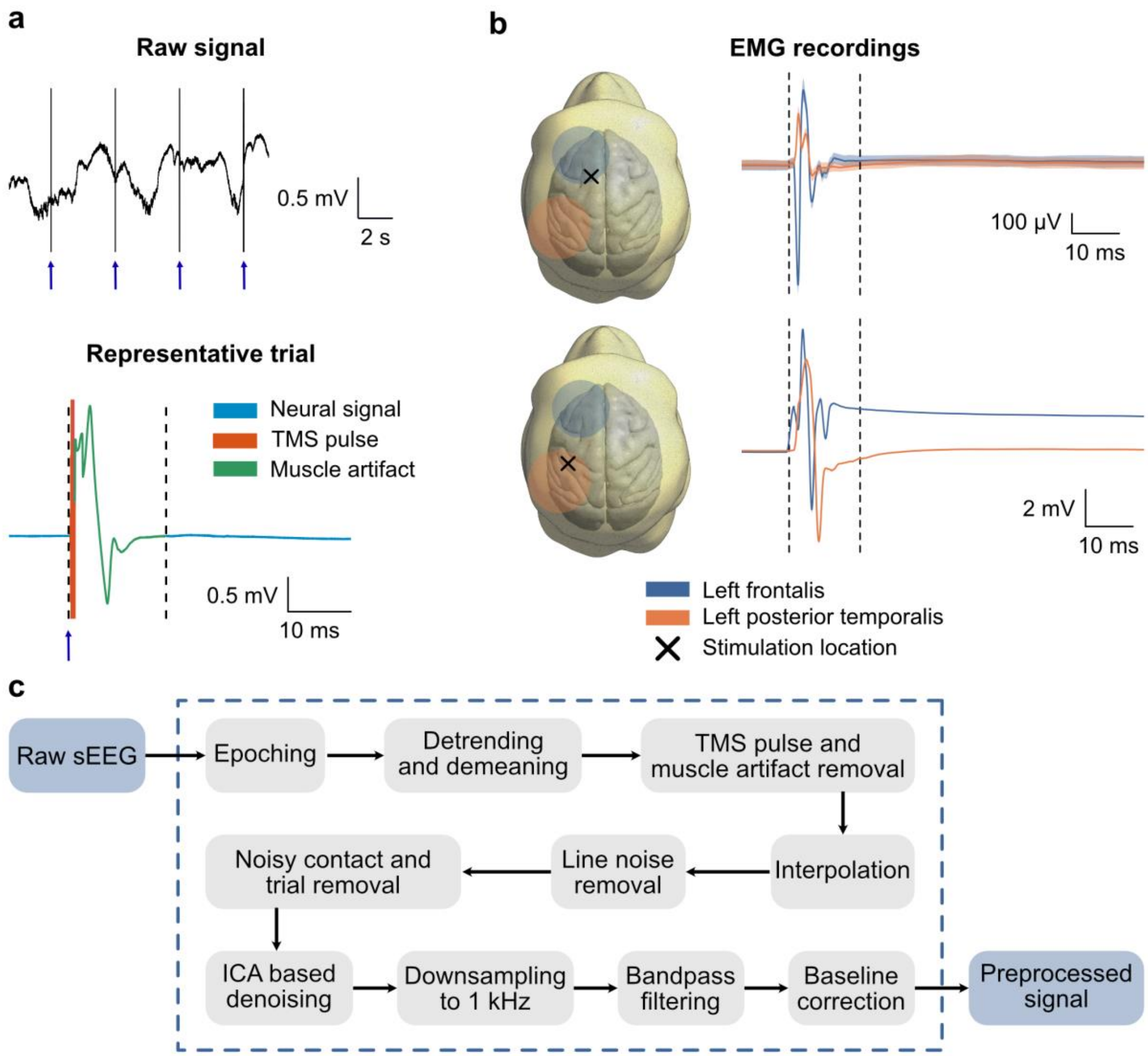

Figure 2.2 Preprocessing of the LFP data. a) Top. A fragment of the raw sEEG signal with TMS pulses marked by arrows. Bottom. A representative trial depicting the presence of TMS pulse, muscle artifact and the neural signal in the sEEG recording. The range of amplitude has been truncated to clearly show the magnitude of the muscle artifact. b) Electromyographic (EMG) recordings obtained by needle electrodes inserted into left frontalis and left posterior temporalis muscles in Monkey W. The general area of the muscle is shaded on the reconstructed head model (blue – left frontalis, orange – left posterior temporalis). Top. Time-locked EMG signals resulting from stimulating frontal brain region. Frontal muscle, that is closest to the stimulation site shows higher EMG activity compared to posterior muscle. Bottom. Time-locked EEG signals resulting from stimulating posterior brain region. In both cases, the muscle activity does not exceed the 15 ms time window that is shown in dashed vertical lines. Stimulation locations are shown by X. Time-locked EEG signals are calculated by interpolating the TMS pulse duration and calculating the average across trials. c) The detailed pipeline used for preprocessing sEEG signals.

Data preprocessing was done in MATLAB (MathWorks® Inc., Natick, MA, USA) using the FieldTrip toolbox (Oostenveld et al., 2011a). The data acquired from the amplifier were preprocessed by separating data into epochs time-locked to TMS delivery (t = 0). The epoch length was 4 s (2 s before and 2 s after TMS delivery). The epochs were then detrended and demeaned. In the next step, we removed the TMS pulse artifact (-0.5 ms to 0.4 ms) and the TMS-induced muscle artifact (0.4 ms to 25 ms in both monkeys) by padding the time windows. The time windows to be excluded were determined by the visual inspection of the LFPs and concurrent electromyographic activity recorded from scalp (see Figure 2.2a and Figure **2.2**b). We interpolated the excluded time window using cubic Hermite interpolating polynomial (pchip) with pre and post data segments of 200 ms. We filtered the resulting LFPs using a bandstop Butterworth filter of order 2 with cutoff frequencies at 57 and 63 Hz. Noisy contacts and trials were excluded through visual inspection. 11 ± 6 (mean ± SD) trials were excluded per experimental block. We performed independent component analysis to manually remove residual artifacts (one component on average per experimental block, maximum of 4). The resulting time series data was then resampled to 1 kHz and bandpass filtered from 1-50 Hz using a 4th order Butterworth filter, followed by baseline correction. See Figure 2.2c for the complete flow of the EEG preprocessing pipeline. We processed baseline data by splitting the traces into 4 s epochs with 50% overlap. We followed the same preprocessing steps for baseline data except for artifact removal and interpolation. For subsequent analysis, we excluded the sEEG contacts located in white matter or outside the brain.

We modeled the electric fields induced by TMS using SimNIBS 3 (Thielscher et al., 2015). We extracted the gray matter and white matter surfaces using a modified Human Connectome Project pipeline for non-human primates (Fair et al., 2020). The surfaces for scalp, skull, and cerebrospinal fluid were created by manual segmentation. Once the complete head mesh was created, we ran simulations for the TMS coil positions used experimentally. We assigned fixed conductivities to each layer: 0.126 S/m (white matter), 0.275 S/m (gray matter), 1.654 S/m (cerebrospinal fluid), 0.01 S/m (skull), 0.465 S/m (scalp) (Opitz et al., 2011). The electric fields were calculated in a quasi-static regime (Thielscher et al., 2011). Through electric field simulations, we sought to visualize the affected brain region and the extent of activation. We computed the robust maximum (99.95th percentile) of the electric field magnitude to remove numerical inaccuracies. To calculate the spatial similarity of electric field distributions on gray matter surface, we first obtained the binary mask by thresholding the electric field magnitude at 50% of the robust maximum. Then, we computed the Sørensen-Dice similarity coefficients on pairs of gray matter surfaces.

2.2.4. Data Analysis

We performed a three-step analysis on the electrophysiological data. First, we analyzed the dose dependency of identified TEPs. Second, we investigated the effect of coil-to-contact distance on the TEP response. Finally, we evaluated the region-specific differences in LFPs and TEP components in the presence of multisensory co-activation.

Following the data preprocessing, we estimated the significance of time-locked LFPs or TMS-evoked potentials (TEPs). The average time-locked activity was calculated for each experimental block. For each stimulation location, we performed a non-parametric cluster-based permutation test (Oostenveld et al., 2011a) ($p < 0.05$) to investigate whether a significant main effect of stimulation intensity is present following TMS (25-400 ms after stimulation pulse) relative to the baseline. The F statistic was calculated for each contact/time pair and clustered according to their temporal adjacency. We used the sum of the F values within a cluster as a cluster-level statistic and compared it against a permutation distribution of 1000 permutations to determine the p value. The highest F value per cluster is reported in Results. The contacts in which the effect was present during at least one stimulation intensity were considered to be ‘responsive’ contacts.

Identified significant TEPs were named according to the timepoint of the maximum deflection (e.g., TEP with the maximum negative deflection at 50 ms is N50). We extracted the N50 component as the minimum amplitude of the LFP in the time window of 40-70 ms from TMS onset, per each trial. To analyze the dose dependency of the TEP components, we extracted N50 for all intensities, from all responsive contacts, and from each stimulation location. TEP amplitudes were normalized to the maximum at each stimulation location. The responses from both monkeys, responsive contacts and stimulation locations were pooled and fit to a four-parameter logistic function,

$$\boldsymbol{\beta_1} + (\boldsymbol{\beta_2} - \boldsymbol{\beta_1})/(\mathbf{1} + (\boldsymbol{\beta_3}/\boldsymbol{x})^{\boldsymbol{\beta_4}}) \tag{2.1}$$

with stimulation intensity as the independent variable and the TEP response as the dependent variable.

Next, we studied the effect of stimulation location on the TEP response through a distance-response relationship. We calculated the Euclidian distances from the TMS coil center projected on the scalp to each electrode contact at each stimulation location. Here, we excluded the contacts without TEP response relative to the baseline (N50 amplitude is within the 99^{th} percentile of the mean LFP amplitude). We assessed the relationship between the distance and response by fitting a linear ($y = a*x + b$) and an exponential decay function ($y = a + b/x^3$). The goodness-of-fit was estimated using adjusted R^2.

Furthermore, we studied the LFPs for the different control conditions. To investigate the peripheral auditory effects, we compared active TMS with and without auditory masking. First, we calculated the averaged total response by combining the trials from all responsive contacts in both tested stimulation locations (locations 1 and 5). To narrow down the auditory and non-auditory responses, we grouped the response of auditory and non-auditory contacts separately and calculated the average response for each condition i.e., masked, and non-masked.

To test whether there’s a statistically significant effect of masking on the TEP responses, we extracted the TEP components from all the trials, and performed Wilcoxon rank sum test ($p < 0.05$) on the total, auditory, and non-auditory TEP responses.

Finally, we studied the effects of auditory click and peripheral somatosensory effects by comparing active TMS, passive TMS and passive TMS + electrical stimulation. Similar to the auditory masking analysis, we calculated the total averaged response from all responsive contacts. Then we grouped the auditory and non-auditory contacts and calculated the average response. To study the effect of auditory click and electrical stimulation on TEP responses, we extracted TEP responses from all contacts and performed Kruskal-Wallis test ($p < 0.05$) on total, auditory and non-auditory TEP responses. We performed follow-up multiple comparisons to evaluate the significant differences across the conditions.

2.3. Results

2.3.1. Dose dependency of TMS Induced Neural Effects

To study the stimulation intensity (dose) dependent effects of TMS on time-locked local field potentials (LFPs), we first identified time windows that showed a significantly different LFP amplitude after stimulation pulse relative to the baseline for at least one stimulation intensity. This was done at five and six separate stimulation locations for two monkeys (named W and H), respectively). The responses were tested using cluster-based permutation test which is a nonparametric test for significance. The TMS-evoked LFPs from both monkeys show a high amplitude activity at ~25-100 ms after stimulation pulse followed by a rebound. In both monkeys, this pattern of activity is conspicuous at the stronger stimulation intensities (≥ 50% of maximum stimulator output, MSO).

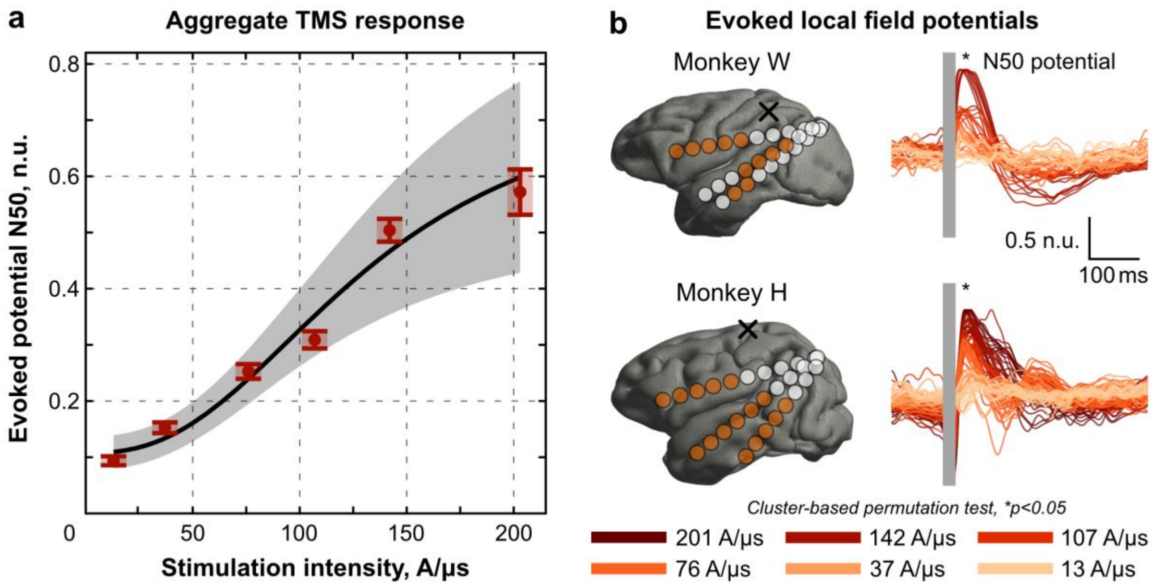

Figure 2.3 TMS-induced early evoked potential N50. a) Aggregated magnitude of early evoked potential N50 in all responsive contacts (significant for at least one stimulation intensity) in both monkeys. The N50 amplitude is normalized per stimulation location per monkey. The curve shows the sigmoidal (logistic) dose-response function with the upper and lower confidence bounds (shaded). The mean squared error of the fit is 0.018. b) Left. The 3D rendering of the brain with the recording contacts (responsive contacts are in dark orange) in both monkeys for a representative stimulation location. Right. normalized local field potentials (LFPs) (overlayed responsive contacts). Responsive contacts were determined by non-parametric cluster-based permutation test, *p < 0.05.

In monkey W, upon stimulation of location 1, three frontal contacts showed significant responses (29-102 ms, F_{max} = 7.93-11.89, p = 0.003-0.037). Stimulation of location 2 showed significance in two frontal contacts (25-99 ms, F_{max} = 6.45-9.53, p = 0.005-0.046). Stimulation of location 3 and 4 resulted in significant responses across four (25-99 ms, F_{max} = 12.36-24.16, p = 9.9×10^{-4} - 0.0017) and five (25-133 ms, F_{max} = 13.27-49.52, p = 9.9×10^{-4} - 0.003) frontal contacts respectively. The contacts mentioned above were located in the corpus striatum and anterior cingulate cortex (see Table 1 for detail). Stimulation location 4 also led to significant responses in the two contacts within the auditory belt (25-91 ms, F_{max} = 19.93-23.92, p = 9.9×10^{-4} - 0.004) and a cluster of four contacts within the superior temporal plane (25-111 ms, F_{max} = 9.35-21.65, p = 9.9×10^{-4} - 0.014). The responses from stimulation location 4 is shown in Figure 2.3b (top). See Figure A.1 and Table 3 for responses from all stimulation locations and summary statistics. In monkey H, the main stimulation locations 1, 2, 4, and 5 showed early latency responses in the contacts that are in the orbitofrontal cortex, corpus striatum, and anterior cingulate. i.e., three contacts in location 1 (25-93 ms, F_{max} = 6.63-12.95, p = 0.0015-0.05), three contacts in location 2 (27-93 ms, F_{max} = 7.39-23.31, p = 9.9×10^{-4}-0.03), three contacts in location 4 (25-130 ms, F_{max} = 8.08-18.25, p = 9.9×10^{-4}-0.042) and five contacts in location 5 (25-133 ms, F_{max} = 12.17-44.03, p = 9.9×10^{-4}). For all main stimulation locations, the contacts in the auditory cortex saw early latency responses (25-145 ms, F_{max} = 6.64-22.61, p = 9.9×10^{-4}-0.045). Locations 1, 3, 4, and 5 also showed significant responses in the contacts in the ventral insular region (25-161 ms, F_{max} = 4.40-18.85, p = 9.9×10^{-4}-0.045). Furthermore, all main stimulation locations resulted in significant responses in the superior temporal and the middle temporal regions while the responses due to stimulating location 5 resulted in longer time windows (Locations 1, 2, 3, and 4: 25-117 ms, F_{max} = 5.46-11.79, p = 0.003-0.041 and location 5: 33-174 ms, F_{max} =

10.03-31.64, $p = 9.9\times10^{-4}$). The responses from stimulation location 5 is shown in Figure 2.3b (bottom). See Figure A.1b and Table 4 for responses from all stimulation locations and summary statistics. The control stimulation location (location 5) in monkey W did not elicit a significant response in the LFPs. However, in monkey H, control stimulation location (location 6) resulted in significant early latency responses in the frontal contacts. The LFPs resulting from stimulating the control location in comparison to its ipsilateral counterpart is shown in Figure A.2a and Figure A.2b for monkey W and H respectively.

In the early latency time windows, the LFPs showed a maximum deflection ~50 ms after TMS delivery. This N50 component demonstrated a pronounced increase in its magnitude with increasing stimulation intensity in the lateral-most stimulation location (locations 3 and 4 in monkey W and locations 4 and 5 in monkey H) in both monkeys. In locations 1 and 2 in monkey W and locations 1, 2 and 3 in monkey H, the N50 component showed a robust response for higher stimulation intensities (90% MSO and 125% MSO). We extracted the N50 component from all responsive contacts across all three electrodes from both monkeys to investigate the dose dependent behavior. The number of total responsive contacts was 20 (3+2+4+11) and 57 (11+10+8+12+16) out of 108 and 135 in monkeys W and H, correspondingly. The N50 components were normalized to the maximum N50 value for each stimulation location. To estimate the overall dose dependency of N50, we fit a four-parameter sigmoid (logistic) curve with TMS dose as the independent variable and the normalized N50 deflection as the dependent variable (Figure 2.3a). The mean squared error of the fit was 0.018.

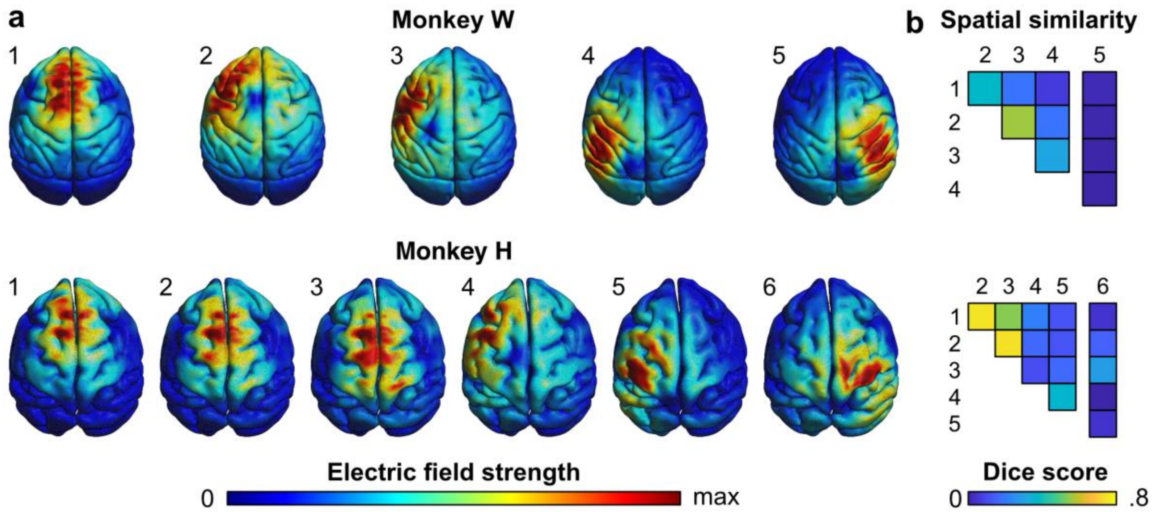

Figure 2.4 TMS-induced electric fields on cortical surfaces. a) The simulations of the TMS-induced electric field strength on the brain surface are shown in Monkeys W and H for each coil location. The electric field strength is color-coded in relative units with respect to the maximum value. In Monkey W, locations 1 (anterior medial) and 2-4 (lateral) constitute main experimental conditions and location 5 is the contralateral control condition. In Monkey H, locations 1-3 (medial) and 4-5 (lateral) are main experimental conditions, and contralateral location 6 is the control. b) The spatial similarity between TMS-induced electric fields as quantified by Sørensen-Dice similarity coefficient. In monkey W (top panel), main stimulation locations demonstrated moderate spatial similarity between pairs (DICE score: 0.19-0.56) while the control stimulation location showed no impact on the recorded hemisphere. In monkey H (bottom panel), the stimulation locations 1, 2, and 3 showed high spatial similarities (DICE score: 0.54-0.75), while the lateral locations 4 and 5 showed moderate similarity between themselves (DICE score: 0.36). The control stimulation location showed little impact on the recorded hemisphere except for stimulation location 3 (DICE score: 0.29).

2.3.2. Effect of Coil Location and Distance-Response Relationship

We performed computational simulations to evaluate the spatial extent of the TMS-induced electric field in the brain under different coil positions (Figure 2.4a). As shown in Figure 2.4b, in monkey W, pairwise Sørensen-Dice similarity coefficient showed anticipated moderate overlap between the main stimulation locations 2-4

(DICE score: 0.19-0.56). In monkey H, the fronto-medial stimulation locations 1, 2, and 3 showed high spatial similarities (DICE score: 0.54-0.75), while the lateral locations 4 and 5 showed moderate similarity between themselves (DICE score: 0.36). The control stimulation location in monkey W showed no impact on the recorded hemisphere (DICE scores with the main stimulation locations < 0.01). In monkey H, the control stimulation location showed little-to-no impact on recorded hemisphere (DICE scores with the stimulation locations 1, 2, 3, and 4 was < 0.15) except for stimulation location 3 (DICE score of 0.29). The recording electrodes were predominantly within the volume of >50% of the maximum electric field magnitude, which we define here as an area of stimulation.

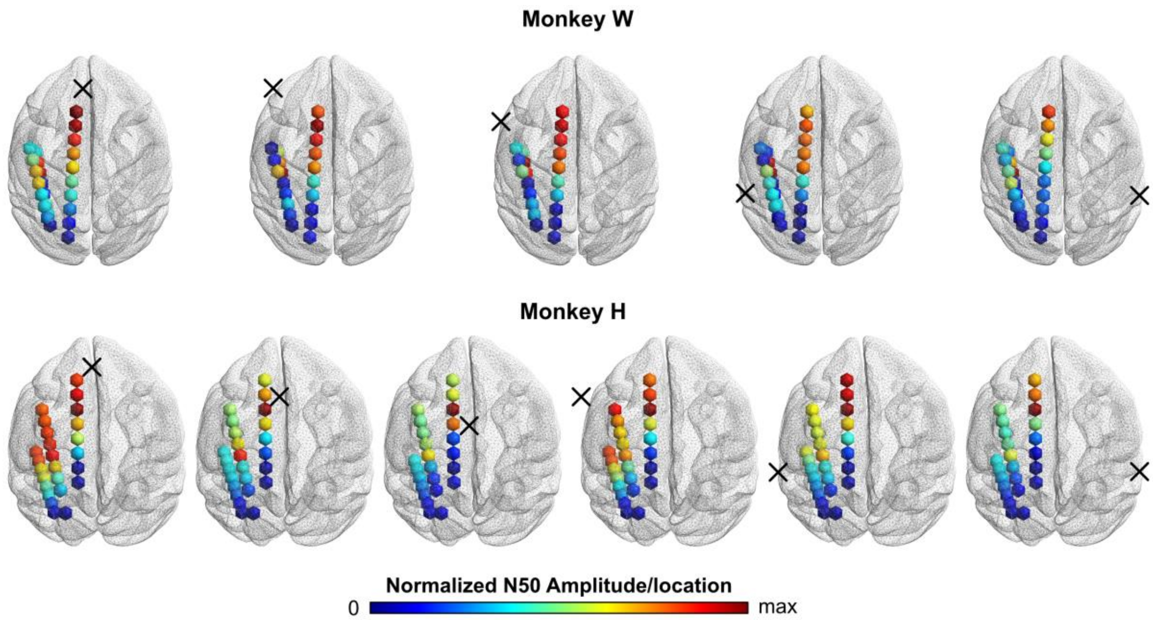

Figure 2.5 Variation of N50 with coil location. N50 amplitude at each contact location is represented by colored dots for each stimulation location (marked as X). The N50 amplitude is normalized to the maximum N50 amplitude for a given stimulation location. N50 amplitudes reported here are for the 90% MSO stimulation intensity.

We visualized the N50 response as a function of the coil location to understand the spatial extent of stimulation using TMS. We normalized the N50 amplitude to the maximum N50 amplitude at each stimulation location. This is shown in Figure 2.5. For fronto-medial and fronto-lateral stimulation locations (locations 1, 2 and 3 in monkey W; locations 1, 2, 3, and 4 in monkey H), we saw increased N50 activity in the most frontal FEF contacts and auditory contacts. In addition, location 1 and 4 in monkey H resulted in increased N50 activity inferior temporal region. Surprisingly, lateral stimulation locations (location 4 in monkey W and location 5 in monkey H) resulted in increased N50 response in the frontal region. Since this distribution of N50 responses is not indicative of the distance between the coil and the contact, we sought to explore whether the coil-to-contact distance drove this variability.

Thus, we explored the relationship between coil-to-contact distance and the N50 response. We focus on the high intensity (90% MSO) condition as it elicits a robust response across most contacts for both monkeys. We combined the stimulation locations 1, 2, and 3 in monkey W and locations 1, 2, 3, and 4 in monkey H for this analysis that were comparable in coil orientation. The lateral most locations (4 in monkey W and 5 in monkey H) were excluded given the different coil orientation. Thus, N = 33 (15+7+11) and N = 49 (14+11+11+13) contacts in both monkeys from the said stimulation locations were included in this analysis. To assess the relationship between the N50 response and the coil-to-contact distance, we fit exponential decay and linear models. A negative linear relationship between the

N50 response and the coil-to-contact distance in monkeys W (R^2-adjusted = 0.51) and H (R^2-adjusted = 0.23) is significant but less accurate than a decaying relationship. The exponential decay fit is much better for monkey W (R^2-adjusted = 0.74) and similar to the linear fit in monkey H (R^2-adjusted = 0.18). The resulting exponential decay fit is shown in Figure 2.6.

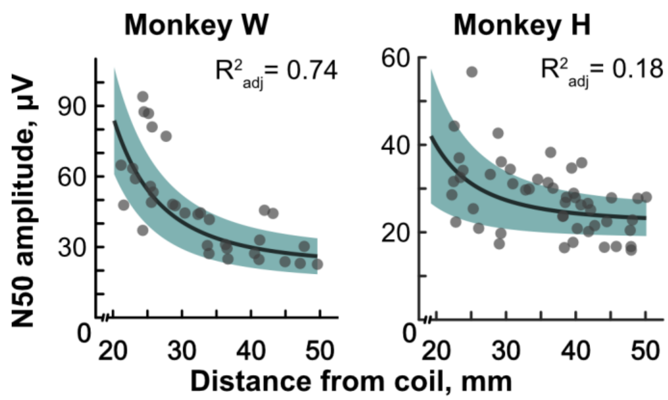

Figure 2.6 Relationship between N50 response and the coil-to-contact distance. Scatter plots show the amplitude of the N50 response against the coil-to-contact distance for each stimulation location. Stimulation locations 1-3 from monkey W and 1-4 from monkey H are included in this analysis. The relationship between the N50 amplitude and the coil-to-contact distance in monkeys W (R^2-adjusted = 0.74) and H (R^2-adjusted = 0.18) show an exponential decay.

2.3.3. TMS-Induced Peripheral Auditory Stimulation Effects

We performed three control experiments to study the effects of peripheral auditory and somatosensory co-stimulation. First, we compared auditory and non-auditory regions during active TMS and active TMS with a masking noise, which suppresses the TMS-associated click sound. For this control, we stimulated locations 1 and 5 in monkey H and extracted LFPs from all contacts that were responsive for both locations. We computed the average LFP responses across all contacts and separately for contacts in auditory and non-auditory brain areas for masked and unmasked conditions separately. The average non-auditory response did not show a visible change between the masked and unmasked conditions. However, the average response and average auditory response show a reduction in amplitude in the early time window in the masked condition compared to the unmasked condition (Figure 2.7a). We further investigated this by extracting the N50 components from the LFPs. The components were normalized to the maximum at each stimulation location. We performed Wilcoxon rank sum test to compare the N50 responses between masked and unmasked conditions for both regions. We found that non-auditory regions are immune to masking ($Z = 1.09$, $p = 0.27$) whereas auditory regions show a significantly lower N50 response during masking ($Z = 5.36$, $p = 8.1 \times 10\text{-}8$). The average response also shows a decreased response when masked ($Z = 3.47$, $p = 5.1 \times 10\text{-}4$). The results suggest that TMS creates centrally-induced effects on neuronal populations in the stimulation area, while also inducing separate response in the auditory cortex due to stimulation click sound.

We compared the effects of auditory click control condition and auditory click with electric scalp stimulation to active TMS (Figure 2.7b). As in the previous section, we considered the total, auditory, and non-auditory responses across conditions. The average LFPs from all three groups showed a pronounced N50 response in the active TMS condition (Figure 2.7b). Click only and click with electric stimulation did not show a pronounced N50 response in the total and non-auditory groups. However, both showed a moderate N50 response in the auditory group that was less than that of the active TMS condition. We performed Kruskal-Wallis test on the extracted N50 responses to test for a significant main effects of stimulation condition (active TMS, click only, and click + electric stimulation). For all three groups, we observed significance (Total: χ^2= 114.68, p = 1.25 × 10^{-25}; non-auditory: χ^2 = 89.15, p = 4.38 × 10^{-20}; auditory: χ^2 = 30.56, p = 2.31 × 10^{-7}) for at least one stimulation condition. Follow-up multiple comparisons tests indicated that active TMS evokes a significantly higher N50 response than both control conditions across all groups. Comparison of total response showed significance for the active TMS vs. click (p = 9.56 × 10^{-9}) and active TMS vs. click with electric stimulation (p = 9.56 × 10^{-9}). Similarly, response in the auditory cluster showed significance for the active TMS vs. click (p = 5.29 × 10^{-5}) and active TMS vs. click with electric stimulation (p = 7.26 × 10^{-7}). Same pairs of conditions were significant in the non-auditory cluster: active TMS vs. click (p = 9.74 × 10^{-10}) and active TMS vs. click with electric stimulation (p = 9.56 × 10^{-10}). This result confirms that the sham protocol used to mimic auditory click and scalp stimulation does not induce TMS effects in non-auditory regions. Furthermore, scalp stimulation did not induce any significant effect on total or non-auditory response, confirming that somatosensory co-activation did not affect the recorded brain regions. In the auditory regions, the auditory click results in N50 response for both control conditions, which is significantly less than in the active TMS condition. This corroborates the observation made in the auditory masking condition that effects on auditory regions include centrally-induced TMS effects as well as peripherally induced effects due to auditory activation.

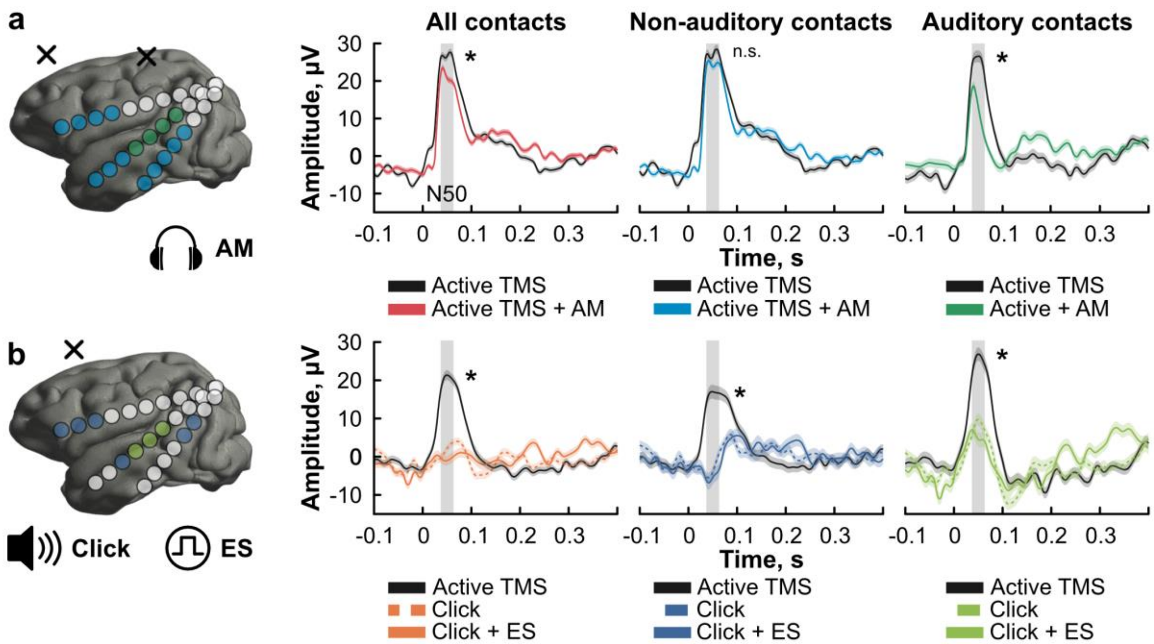

Figure 2.7 Centrally-induced TMS neural effects are separable from peripheral auditory and somatosensory activation. Total average response, average non-auditory response, and average auditory response are calculated from the responsive contacts. The responsive contacts are shaded in blue (non-auditory) and green (auditory). The TMS coil locations are indicated by X above the cortical surface. The N50 responses are extracted on a trial basis for comparison across controls. a) Auditory masking results in diminished N50 response localized to the auditory region when active TMS is delivered. The Wilcoxon rank sum test indicates significantly lower N50 response in the average response ($p = 5.1 \times 10^{-4}$). When the responses are clustered into auditory and non-auditory regions, the same test indicates that the N50 response in the auditory region shows a significantly lower response ($p = 8.1 \times 10^{-8}$) in the masked condition compared to unmasked when delivering active TMS. The test returns no significant difference for the N50 response between masked and unmasked conditions in the non-auditory regions. b) Auditory click and auditory click + electrical stimulation do not induce N50 responses comparable to active TMS. Kruskal-Wallis tests for N50 component for total response, non-auditory response and auditory response showed a significant difference across the three conditions (Total: $\chi^2 = 114.68$, $p = 1.25 \times 10^{-25}$, Auditory: $\chi^2 = 30.56$, $p = 2.31 \times 10^{-7}$, non-auditory: $\chi^2 = 89.15$, $p = 4.38 \times 10^{-20}$). Follow-up multiple comparisons tests revealed that the total N50 response was significantly different for the active TMS vs. click ($p = 9.56 \times 10^{-9}$) and active TMS vs. click with electric stimulation (ES; $p = 9.56 \times 10^{-9}$). The auditory N50 response was also significantly different for the active TMS vs. click ($p = 5.29 \times 10^{-5}$) and active TMS vs. click with ES ($p = 7.26 \times 10^{-7}$). A similar observation was made on

non-auditory N50 response where the active TMS vs. click ($p = 9.74 \times 10^{-10}$) and active TMS vs. click with ES ($p = 9.56 \times 10^{-10}$) were significantly different. n.s. = not significant, *$p < 0.05$.

2.4. Discussion

We investigated how single-pulse transcranial magnetic stimulation (TMS) affects mesoscale level neuronal activity in non-human primates depending on TMS intensity and coil position. Further, we employed several control conditions to dissociate the target effects in the brain from peripheral auditory and somatosensory side effects. We found that early evoked potentials, occurring ~50 ms after TMS pulse, characterize a centrally-induced neural response to stimulation that could be a result of local suprathreshold activation in neuronal populations or connectivity to cortical brain regions more proximal to TMS. These early local field potentials demonstrate a characteristic, sigmoidal dose-response dependency and inversely relate to the distance from the brain area to the stimulation coil. This centrally-induced brain response is well dissociable from acoustic co-stimulation, particularly evident in the auditory cortex, and somatosensory co-stimulation, which doesn’t induce specific early evoked components. These findings provide the basis for concurrent TMS-EEG studies in humans and put forward early evoked potentials as a clinically-relevant target engagement biomarker.

We found that TMS stimulation results in TEPs characterized by high amplitude and short latency. In both monkeys, the early activity expressed itself as a positive peak at ~50 ms. In monkey W, we saw a later rebound component at the highest stimulation intensity. Comparable observation has previously been reported in TMS-EEG studies in humans in unconscious or anesthetized states (Ferrarelli et al., 2010; Massimini et al., 2005; Sarasso et al., 2015). During such states, the TEPs are localized to the stimulation region, which results in less complex brain activity. However, in attentional states, the long-range brain connectivity results in complex TEPs with multiple peaks. The early response we observed here was robust in several brain areas across multiple TMS coil locations. While fronto-medial stimulation locations are only effective at high doses (e.g., 90% MSO), lateral stimulation locations showed a characteristic, sigmoidal dose-response dependency with increasing TMS intensity. In particular, we found that early LFP component (N50) captures a mesoscale brain response not reported in the non-human primate literature so far. Nevertheless, the effects of single pulse TMS on the visual cortex of anesthetized cats have been studied with electrophysiological recordings and optical imaging (Kozyrev et al., 2014; Moliadze et al., 2003). While these studies provide important insights into complex TEPs patterns, research in non-human primates enables straightforward translation to humans (Alekseichuk et al., 2019). Two groups have studied the effects of TMS on the microscale neuronal level in non-human primates. One group examined single unit activity during stimulation in different types of neurons (Mueller et al., 2014). Example neurons showed bursts of activity at short latencies (< 100 ms), especially around 50 ms. The other group showed that the majority of single units demonstrated increased short latency (10 – 40 ms after TMS delivery) spiking activity in parietal neurons during task-related activity, while some neurons demonstrated excitation-inhibition-excitation pattern (Romero et al., 2019). While the summation of single neural firing should result in the population-level response, our study directly shows the aggregate LFP activity in neural circuits and its potentiation approximately 50 ms after TMS delivery. Hence the N50 component captures direct physiological effect of TMS.

To ensure that the TEPs are not a consequence of currents induced by inductive loops in the recording setup, we ensured that the contacts of the electrodes and the electrical cables were free of loops. Furthermore, the high input impedance of the amplifier results in negligible currents compared to the biological currents that gives ride to the LFPs. An interesting question is whether the TEPs observed here are due to direct suprathreshold neural stimulation at the recording sites or propagated from more superficial brain areas via neural circuits, or both. The TMS-induced electric fields have maximum strength at the neocortex; however, a substantial part of the electric field in the small NHP brain also reaches deeper areas. In addition, the absolute field values necessary to induce suprathreshold neural activation in the brain are unknown to date. Thus, we focus our analysis on the relative values of electric field magnitude. Electric field modeling cannot directly distinguish between the abovementioned possibilities, which remain an exciting avenue for future research.

We also observed that the lateral-most stimulation locations in both monkeys (location 4 in W and location 5 in H) showed activation in the distal contacts compared to the proximal ones. We speculate that this could be due to a couple of reasons: 1) The coil orientation used for these two locations were different from the rest due to the headpost placement, which could have resulted in activation of deeper, frontal regions and 2) The lack of activation in the proximal contacts could be due to the placement of some of these contacts in the WM (or WM and GM interface – refer Tables 1 and 2). We did not observe the same LFPs in these contacts and they were excluded from the analysis. Monkey H's brain presented a variant brain anatomy, particularly in the parietal and occipital neocortical regions. Given that we operated outside these areas and normal daily behavior demonstrated by this NHP, we consider the recorded TEPs in Monkey H as normal. The similarity of TEP components observed in both monkeys further validates our designation.

Dose selection is a vital ingredient in TMS application, whether in research or therapy. Rational dose selection enables achieving desired treatment outcomes (Herrmann et al., 2006), and eliciting desired activity in the brain when probing brain networks. Coupling the stimulation dose with a biomarker that reflects neural activity centrally-induced by TMS is a key prerequisite for developing optimized dose control. In human TMS studies targeting the motor cortex, the effect of TMS stimulation intensity has mostly been studied using motor-evoked potentials (MEPs) (Darling et al., 2006). Given that MEPs are an indirect readout of cortical reactivity in the form of a muscle response, the effects of TMS intensity can be quantified easily. However, in brain regions pertaining to cognitive processes, for example, prefrontal or parietal cortex, such dose-response relationships have not been established with easily accessible readouts. In such cases, TEPs can serve as important biomarkers that explain the effects of stimulation intensity and connect them with behavioral responses. In previous human work, the intensity dependency of TEPs in human PFC was demonstrated using TMS-EEG (Kähkönen et al., 2005). However, this study was limited to a single brain region and did not disentangle centrally-induced TMS effects from multisensory co-activation.

We used electric field simulations to study the effect of coil position on the field distribution. The Sørensen-Dice similarity coefficient analysis indicated similarity in electric field distributions between stimulation locations that are on the hemisphere ipsilateral to recording electrodes. The smaller size of the monkey brain and the range of coil movement that was ≤ 3 cm between adjacent stimulation locations, lead to overlapping field distributions. Control location 5 in monkey H scarcely overlapped with distributions from other locations. However, in monkey H, two medial stimulation locations had overlapping distributions with the control location. Furthermore, the electric field distribution when stimulation location 6 in monkey head also showed electric fields reaching the medial electrode in the left hemisphere. This can explain the response we observed in LFPs when stimulating location 6. As the monkey brain is considerably smaller than the human brain, the percentage of the brain volume activated by TMS is higher in monkeys than in humans (Alekseichuk et al., 2019). Thus, the spatial specificity of TMS is likely reduced to what would be expected in humans.

Investigating the spatial dependency of TEP responses, we observed a relationship between the N50 amplitude and the distance from the TMS coil to the recording contact. An inverse linear model and an exponential decay model can explain the seen relationship. Yet, the decay model captures this effect better, especially in monkey W. This observation agrees with the nature of the magnetic field, which is rapidly decaying in magnitude with increasing distance from its source.

The effect of coil-to-cortex distance on TMS effects on DLPFC (Nahas, Teneback, et al., 2001) and motor cortex (McConnell et al., 2001; Stokes et al., 2007) has been studied previously across subjects. While Romero et al. (Romero et al., 2019) showed that TMS elicits spiking activity with a very high spatial specificity, we observed more widespread neural effects on the brain. The key differences in this study and our study potentially led to different observations: I) Their stimulation paradigm is limited to one brain region, hence is limited in explaining effects arising from stimulating other regions, II) they record from a single brain region and therefore cannot capture the induced effects that are propagated to connected regions, and III) the difference of the scale of recording, i.e., single units vs neural circuits.

We incorporated several control conditions to disentangle centrally-induced neural effects from peripheral sensory effects. We conclude that auditory masking only affects the response in auditory regions confirming that a fraction of the response due to TMS is in fact auditory evoked in nature. Similarly, the difference of responses in active TMS and passive TMS (auditory click) conditions confirms the above observation. We did not observe a visible response in non-auditory regions during passive TMS. Electrical stimulation of the scalp (coupled with passive TMS) to control for somatosensory activation did not produce a significant response in the non-auditory regions. Since the depth electrodes did not have contacts in the somatosensory cortex, we could not determine whether a response localized to that region was present during electrical stimulation. The evoked potentials we observed during passive TMS and electrical stimulation did not elicit long latency responses. In fact, the somatosensory evoked potentials in anesthetized monkey preparations have shown to be short latency in nature and lasting up to 25 ms (Allison et al., 1991). Therefore, it should not impact our findings in the responses appearing after 25 ms. Research of different anesthetics in humans shows the normal modulation of middle latency auditory evoked potentials at 10-100 ms after stimulus delivery (Goto et al., 2001). These modulatory effects are also shown for somatosensory sensation (Sparks et al., 1975). Hence, our analysis is confined to the TEP components that show modulatory effects for the given conditions. Present results have implications in TMS-EEG studies. Interpreting TEP components and assessing their origins is challenging due to limitations of EEG recordings (Conde et al., 2019). A recent study has attempted to disentangle peripheral activations from centrally-induced TMS effects using similar controls (Rocchi et al., 2021). The study has compared the TEPs across conditions in the vicinity of a single stimulation site. Despite similar observations being made on modulation early evoked activity, direct recordings from auditory regions in our study give us valuable insights about centrally- and peripherally-induced TMS effects on auditory and non-auditory regions.

The main TEP component we observed in this study can be compared with some of the human TMS-EEG studies. Several human TMS-EEG studies have reported N100 response resulting from stimulation in the vicinity of M1 (Bikmullina et al., 2009; Kičić et al., 2008). The N100 component has also been observed in TEPs resulting from prefrontal cortex stimulation (Kähkönen et al., 2005; Rogasch et al., 2015). This component has been implicated as a neurophysiological marker of cortical inhibition through MEP measurements (Kičić et al., 2008; V. V. Nikulin, Kičić, et al., 2003). The disparity in latency could be attributed to the differences in neural dynamics, gross functional anatomy and cellular physiology between humans and monkeys (Paller et al., 1992). However, there is also evidence for TMS evoked responses in humans that are commonly characterized by early potentials such as cortical N40 and occur on the same timescale as we observed here (Casula et al., 2014; Kerwin et al., 2018). Importantly, the distinction between recording modalities also contributes to differences in latency. Furthermore, using anesthetized preparations of non-human primates also contributes to such differences. In human literature, several TMS-EEG studies reveal complex TEP waveforms during attentional states. These include peaks at 15, 30, 45, 60, and 100 ms during motor cortex stimulation (Ilmoniemi & Kičić, 2010; Rogasch & Fitzgerald, 2013a) and peaks at 27, 40, 60,100, and 180 ms following prefrontal stimulation (Kähkönen et al., 2004; Lioumis et al., 2009). However, in sleep or unconscious states, the TEP components are less complex, more localized, and higher in amplitude (Ferrarelli et al., 2010; Massimini et al., 2005; Sarasso et al., 2015). We observe response patterns in two anesthetized monkeys equivalent to the sleep or unconscious findings in humans. Furthermore, the human data on subcortical ERPs is very scarce and it is not clear if the subcortical ERP we observed here is more or less complex than its human counterpart. While TMS induced effects are state dependent, anesthetized models still provide important mechanistic understanding about neural effects induced by TMS. Previous studies have used anesthetized monkey models to explain the activity of visual cortex when presented with visual stimuli (Logothetis et al., 1999) and effects of repetitive TMS using functional imaging (Hayashi et al., 2004; Ohnishi et al., 2004). Nevertheless, future work is needed to establish N50 as a biomarker in humans and the present work lays significant advances towards this goal.

Conclusion

Understanding the relationship between TMS dose and physiological responses is crucial for optimizing TMS parameters to achieve desired clinical outcomes, elicit network activity, and induce plasticity. Furthermore, understanding the origins of evoked components in non-invasive EEG and the correct interpretation of TEPs in the presence of multisensory coactivation improve their utility as biomarkers for target engagement. Our study provides important findings regarding the dose-dependent physiological effects of TMS, the role of stimulation location and the distance between the target brain region and the coil position, and the impact of multisensory coactivation due to TMS on evoked potentials. Together, present results provide a mechanistic basis for human TMS-EEG studies and TMS biomarkers for clinical therapy.

The work discussed in this chapter is published in the Journal of Neuroscience (N. D. Perera et al., 2023).

Chapter 3: Effects of State-Dependent TMS on EEG Biomarkers in Humans

3.1. Introduction

The brain is dynamic in nature, meaning that neural, regional, and metabolic activity is changing in each moment. Consequently, the current state of the brain determines physiological and behavioral output. Neural oscillations that can be measured from the scalp using electroencephalography (EEG) reflect how the state of the brain is modulated. Such oscillatory activity, which offer an approximation of local field potentials, fluctuates in a rhythmic manner and can be categorized in several frequency ranges of interest. Therefore, the phase of a neural oscillation is an indicator of the brain state (Berger et al., 2014; Combrisson et al., 2017; Miller et al., 2012; O'Keeffe et al., 2020). External stimulation at different oscillation phases will thus result in variable levels of brain excitability, however, the exact relationship between oscillation phases and brain excitability is not fully understood.

Recent advances have allowed for testing the causality between oscillation phase of the mu (8-13 Hz) and beta (14-30 Hz) rhythm and cortical excitability in the primary motor cortex (M1). For this, transcranial magnetic stimulation (TMS), which activates the corticospinal tract from M1 to a target muscle, is triggered at a particular oscillation phase that is obtained from a real-time read-out and analysis of EEG. Studies using real-time TMS-EEG have demonstrated and replicated that M1-muscle corticospinal excitability depends on oscillation phase (Bergmann et al., 2019; Karabanov et al., 2021; Madsen et al., 2019; Zrenner et al., 2018). While the trough and rising phase of the mu rhythm results in the largest activation by TMS, the peak and falling phase predicted the largest activity for the beta rhythm. While these findings deepen our fundamental understanding of neural physiology, they also have clinical relevance. Repetitive TMS is an FDA-approved method to treat psychiatric and neurological disorders, yet its efficacy is variable. Real-time TMS-EEG could overcome this variability by consistently targeting the optimal oscillation phase.

While previous findings have shed light on the relation between oscillations and brain excitability, our understanding remains incomplete. Specifically, corticospinal excitability is measured by investigating a TMS-induced muscle response, referred to as a motor-evoked potential (MEP). As such, this method is restricted to the motor cortex and is unable to study phase-dependencies in other parts of the cortex. Furthermore, while they are indicative of cortical activation, MEPs are confounded by background activity fluctuations at the spinal and muscle level. To overcome these limitations, the phase-specific effects of TMS can be measured directly on EEG potentials as TMS-evoked potentials (TEPs). In addition, TEPs can be recorded from other locations on the scalp and can thus be used for nonmotor regions as well. TEPs reflect a broad range of activity in the targeted brain region. Early TEPs in the motor cortex, for example, N15, reflect direct cortical activation of the motor/premotor area (Esser et al., 2006; Litvak et al., 2007; Mäki & Ilmoniemi, 2010). The later components such as P50 and N100 may reflect reafferent activity and secondary effects from multiple sources (Desideri et al., 2019; Mäki & Ilmoniemi, 2010; Petrichella et al., 2017; Roos et al., 2021). Previous non-human primate studies by our group have shown these direct and peripherally induced TMS effects can be dissociated using invasive electrophysiology (N. D. Perera et al., 2023) highlighting their potential to measure direct cortical responses to TMS. Currently, there is sparse evidence for the effects of oscillation phase on TEPs. One study showed a phase-dependent modulation of early and late TEP components (e.g. P60/P70 and N100) during peak and trough phases of the mu rhythm (Desideri et al., 2019). TEPs in the beta rhythm have not been investigated so far to our knowledge.

The goal of the present study is I) to systematically investigate the causal relationship between cortical activation, as measured by TEPs, and oscillation phase in the mu and beta rhythm; and II) to directly compare the effects of real-time phase-dependent TMS on cortical activation, as measured by TEPs, and corticospinal excitability, as measured by MEPs. Our results indicate phase-dependent modulation of early and late TEP components in both mu and beta oscillations. Furthermore, corticospinal excitability and cortical activity follow a 90^0 out of phase relationship for mu oscillation while beta did not show a quantifiable relationship. Our results indicate the possibility of distinct mechanisms that modulate corticospinal excitability and cortical responses in the sensorimotor cortex. This is important when developing biomarkers of brain function and excitability, an important consideration in clinical outcomes at large.

3.2. Materials and Methods

3.2.1. Participants, Real-Time TMS Triggering and Data Acquisition

We recruited 20 healthy volunteers for this study (11 female, mean ± std age: 22.7 years ± 2.9, range: 18-45 years). All participants were right-handed and without reported history of neurological or psychiatric disorders. The study was approved by the institutional review board of the University of Minnesota and all participants were consented prior to participation in the study. The reader is referred to Wischnewski et al. for additional information on the dataset used in this study (Wischnewski et al., 2022).

We used Magstim Rapid^2 stimulator with a figure-of-eight D70^2 coil (Magstim Inc., Plymouth, MN, USA) to deliver single pulse TMS. We recorded electromyography (EMG) from the right first dorsal interosseus (FDI) muscle using BIOPAC ERS100C amplifier (BIOPAC systems Inc., Goleta, CA, USA). Initially, the coil was oriented at 45^0 relative to the midline and the hotspot was determined as the coil location and orientation eliciting the highest motor evoked potential (MEP). Once the hotspot was located, the coil location and orientation were continuously tracked using Brainsight neuronavigation system (Rogue Research, Montreal, Canada).

The resting motor threshold (rMT) was determined based on maximum likelihood parameter estimation by sequential testing (PEST) (P. Julkunen, 2019). For the subsequent real-time TMS, the intensity was set to 120% rMT.

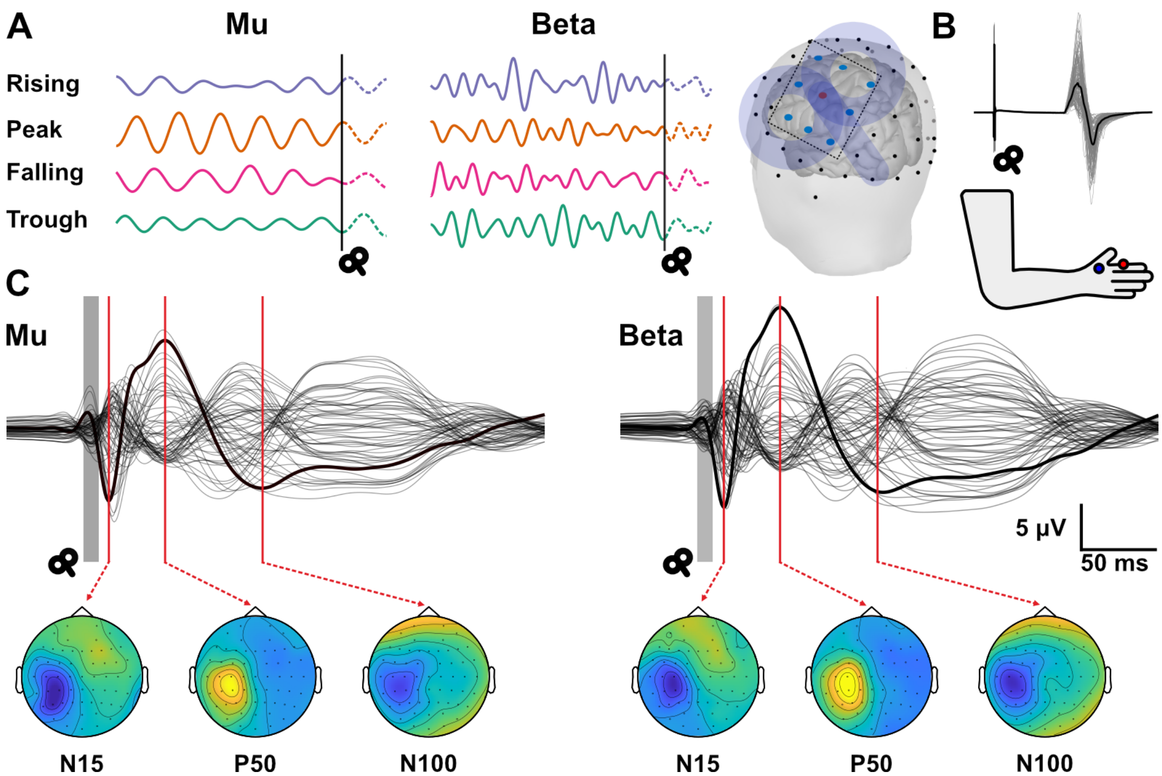

Figure 3.1 The overview of phase and frequency targeting, and TMS evoked potentials (TEPs). A) An example of phase targeting during the training phase of the educated temporal prediction (ETP) algorithm. ETP algorithm accurately targets rising, peak, trough and falling phases of both mu and beta frequency bands. The rendering of the brain shows the Laplacian montage of the electrodes (FC5, FC3, FC1, C5, C1, CP5, CP3, and CP1) used to extract the C3 signal. The coil was placed on the motor hotspot corresponding to first dorsal interosseus (FDI) muscle. B) Example of motor evoked potentials (MEPs) acquired from FDI muscle for a single participant with bold trace representing the mean MEP. Bottom panel shows the montage used for EMG acquisition from FDI muscle. C) The global average TEP signal for each target frequency band. The bold trace indicates the C3 signal. The topography of the three components, N15, P50 and N100 used to characterize cortical responses are shown below each trace.

We recorded the EEG using 64-channel actiCAP Slim active electrodes and actiCHamp EEG amplifier (Brain Products GmbH, Gilching, Germany). For this study, we used the educated temporal prediction (ETP) algorithm (Shirinpour et al., 2020) to stimulate rising, peak, falling, and trough phases of sensorimotor mu (8-13 Hz) and beta (14-30 Hz) oscillations. The ongoing oscillation for phase targeting was calculated as the Laplacian C3 signal with 8 surrounding electrodes (FC1, FC3, FC5, C1, C5, CP1, CP3, and CP5). Resting state EEG was acquired for 3 minutes immediately prior to the stimulation to train the ETP algorithm. Subsequently, the same Laplacian C3 signal was used for real-time TMS triggering, while ongoing EEG activity was recorded and saved at the end of each experiment session (Figure 3.1A).

Each participant underwent two separate experiment sessions for targeting mu and beta oscillations. The sessions were at least 48 hours apart to prevent carryover effects and were randomized across participants. During each experiment session, the participant received a total of 600 pulses, in four blocks of 150 pulses. In each block, the phases were targeted pseudorandomly, where both the experimenter and the participant were blinded to the target phase. The pulses were delivered with a jitter of 2-3 s to prevent the effects of last pulse on the current pulse.

3.2.2. Electrophysiological Data Preprocessing

The MEPs were extracted from a window of 20-60 ms following TMS pulse. MEPs were considered noisy if the average absolute baseline EMG activity (-100 ms to

0 ms relative to TMS pulse) was above 0.02 mV and larger than absolute average EMG activity + 2.5 times standard deviation of resting state EMG. sufficiently deviated from a predefined threshold. For each subject, the individual MEPs were normalized to the average of all MEPs.

EEG data was preprocessed using custom scripts in MATLAB (MathWorks Inc., Natick, MA, USA) using FieldTrip toolbox (Oostenveld et al., 2011b). The raw EEG data from 4 blocks was combined into one block of 600 trials. This EEG data was separated into epochs between -1 s and 1 s, time-locked to TMS trigger (t = 0). The data was then demeaned and detrended, and the pulse artifact and early muscle activity between -6 ms and 10 ms was removed by padding the time window. The excluded time window was then interpolated using the cubic Hermite interpolating polynomial (pchip). The bad channels and trials were then removed by visual inspection. On average, 6.6% of the trials for targeting mu and 8.0% of the trials for targeting beta were removed (7.3% trials removed from the total number of trials). On average, one channel was removed from each session for each participant. We performed independent component analysis (ICA) to remove residual muscle activity, and ocular artifacts using the infomax ICA algorithm (Bell & Sejnowski, 1995) implemented in FieldTrip. On average, 6.7 components were removed from mu session and 6 components were removed from beta session. The data was then resampled to 1 kHz and bandpass filtered between 1 and 50 Hz using a 3rd order Butterworth filter. We interpolated the channels using spline interpolation of neighboring channels. The definition of neighboring channels was acquired from the default template available in FieldTrip for the EEG cap used in the experiment. Finally, the data was referenced to the common average and baseline corrected with a window of -500 ms to -15 ms.

Once EEG data was preprocessed, we clustered the trials based on the targeted phase and calculated the average TMS evoked potentials by averaging across trials. We identified the TEP components that are commonly reported in literature, N15, P30, P60, and N100 (Ilmoniemi & Kičić, 2010). While N15 and N100 were consistent, the prominence of P30 and P60 peaks varied across participants (Figure 3.1C). Some participants showed a pronounced P30-N45-P60 complex, while the others showed either P30 or P60. For our analysis, we extracted the peak TEP components from predefined time windows of interest, 10–20, 20–70 and 90–130 ms. In the 20–70 ms window, we extracted the most prominent peak in each participant. We called these M1 TEP peaks, N15, P50 (despite the variation of latency in the 20–70 ms time window), and N100. Given that these evoked potentials are noisy in the trial level, we defined N15 potential as the mean amplitude 15 ± 2 ms after the TMS pulse, P50 potential – 50 ± 5 ms, and N100 potential – 100 ± 10 ms for the trial level analysis of TEP components. These windows were chosen considering the prominence of the peaks.

Pre-TMS power spectrum of C3 electrode was calculated to investigate whether pre-stimulus activity correlates to post-stimulus evoked activity. We did so by applying fast Fourier transform with a single Hanning taper at a resolution of 1 Hz on the time window between -550 and -50 ms. Pre-TMS mu and beta power were calculated as the mean power in the 8-13 and 14-30 Hz range respectively.

3.2.3. Interpretability of TEPs in a Phase-Locked Paradigm

The interpretation of TEP components when TMS is delivered at a specific phase repetitively, comes with a limitation. While the time-locked averaging procedure cancels out background EEG activity, phase-locked activity survives. The amplitudes of TEP components could be interpreted only if TMS causes transient phase resetting of the ongoing oscillation. If such a transient phase reset does not occur, a correction could be applied by creating phase-locked non-stimulated trial and channel-wise subtraction of phase-locked non-stimulated average from phase-locked stimulated average (Bergmann et al., 2012; Desideri et al., 2019; Kruglikov & Schiff, 2003). We tested whether a transient phase reset occurs during TMS using the measure, phase preservation index (PPI) (Desideri et al., 2019; Mazaheri & Jensen, 2006). The PPI is calculated by the following equation:

$$PPI(c,f,t) = \frac{1}{n}\left|\sum_{k=1}^{n} e^{i(\varphi_k(c,f,t_{ref})-\varphi_k(c,f,t))}\right|$$

where c denotes a channel, f denotes the frequency of interest, t denotes the time point, $\varphi_k(c,f,t)$ is the phase of frequency f at time point t, for the k^{th} trial of channel c and t_{ref} is a reference time point before the stimulus. For mu-specific targeting, t_{ref} was chosen to be 200 ms before stimulus delivery and for beta-specific targeting it was 100 ms. The shorter t_{ref} for beta was due to the nonstationarity of beta compared to mu oscillations. We performed this by offline targeting of phases on the resting data to create non-stimulated trials in 18 sessions out of 40 (9 per mu and beta). The resting data for the other 22 sessions was not available due to an error related to saving data. However, we did not find conclusive evidence for stability of phase following TMS delivery (Figure A.3 and Figure A.4). Since we cannot conclusively prove that phase is reset during TMS, we utilized peak-to-peak amplitudes of TEP components to quantify the cortical responses. Therefore, we considered two TEP complexes in our study, P50-N15 (early response) and P50-N100 (late response).

3.2.4. Statistical Analysis

In group level analysis of the TEP amplitudes, repeated-measures analysis of variance (rmANOVA) was performed on target phase and rhythm. This was followed by multiple comparisons tests to investigate pairwise differences according to Tukey HSD correction.

To investigate the relationship between TEP and MEP relationship, we used a preferred phase approach. We did so by reducing the electrophysiological measures to two orthogonal components (peak-trough and fall-rise). We then calculated the resultant magnitude and direction by converting the two orthogonal components into polar coordinates. To test whether MEP and TEP components have a predictable phase dependency, we calculated the phase difference between the preferred phase of MEP and TEP components. A phase difference of 0^0 would result in a similar phase relationship, whereas a phase difference of 90^0

would mean an opposite relationship. We calculated this between MEP and each TEP component for each participant.

To study the effect of pre-TMS band power on TEP components, we ran generalized linear mixed-effect models on trial level each target band. We considered the target phase (rising, peak, falling, trough) and target pre-TMS band power as fixed effects, and participant number as random effect. On the group level, we studied the relationship between pre-TMS power and average TEP amplitude by calculating Spearman's rank correlation.

We further investigated how the interaction of pre-TMS mu and beta power affect the cortical responses. We pooled TEP and power data from all trials (from both mu and beta target sessions) and performed a median split on the mu and beta power separately for each participant. Next, we classified the trials into four classes as mu high-beta high, mu high-beta low, mu low-beta high, mu low-beta low. Finally, we calculated the class average of early and late responses for each participant and normalized it to the subject average. We performed Wilcoxon signed rank test to compare the classes in a pairwise manner. An additional analysis was performed on pre-TMS delta and theta rhythms separately using the same approach. This was done to verify that TEP responses are not modulated by the pre-TMS delta and theta power. For all analyses, the significance level was set to be $\alpha = 0.05$.

3.3. Results

3.3.1. Phase Dependent Modulation of Cortical Responses

First, we quantified the early (P50-N15) and late (P50-N100) peak-to-peak TEP complexes in the time-locked averaged signal per participant. TMS delivered at specific phases of oscillations shows differential modulation of cortical responses, dependent on target phase and oscillatory frequency. We observed that mu-specific targeting resulted in larger amplitude changes in early (0.95 – 1.06 n.u.) and late (0.97 – 1.03 n.u.) cortical responses. Comparatively, beta-specific targeting resulted in lesser changes in early (0.98 – 1.02 n.u.) and late (0.99 – 1.01 n.u.) cortical responses (Figure 3.2). This suggested generally stronger effects at the mu rhythm. Similarly, the early response showed larger phase dependent modulations compared to the late response for both target rhythms.

Next, we investigated the effects of target phase and target rhythm on the early TEP component. At the group level, rmANOVA showed a significant main effect of target phase [$F(3, 57) = 6.96$, $p < 0.001$] and a significant target phase × target oscillation interaction ($F(3, 57) = 5.96$, $p = 0.001$) on the early TEP component. When mu-specific target is considered, trough to falling phases showed increased modulation (1.03 – 1.06 n.u.) of cortical early response. Conversely, peak and rising phases showed decreased modulation (0.95 – 0.96 n.u.). The difference between increased and decreased modulation was statistically significant (post-hoc multiple comparisons test with Tukey HSD correction; $p < 0.02$). During beta-specific targeting, the early response showed increased modulation at rising phase (1.02 n.u.) and decreased modulation at peak phase (0.98 n.u.). The difference between these phasic modulations was significant (p = 0.02).

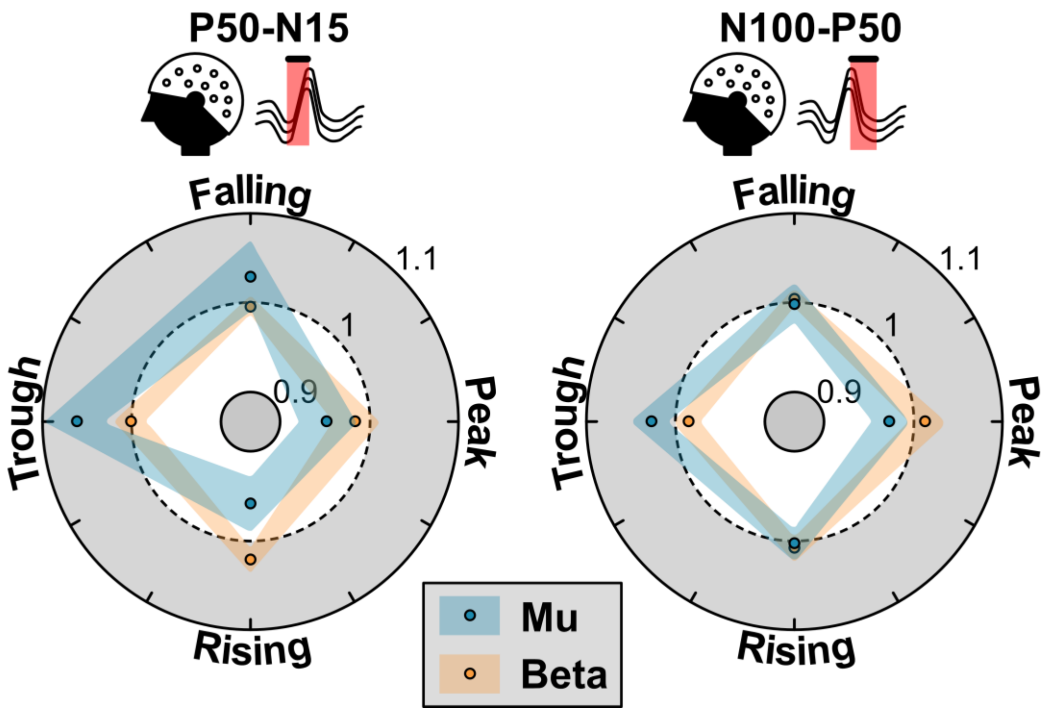

Figure 3.2 Phase dependency of TEP components for mu and beta rhythms. Left: Phase dependency of the early component, P50-N15. Mu target rhythm showed significant increased modulation of TEP amplitude for trough and falling phases compared to peak and rising ($p < 0.02$). For beta target rhythm, rising phase showed significantly higher TEP amplitude modulation compared to peak phase ($p = 0.02$). Right: Phase dependency of the late component, P50-N100. The late component showed opposite amplitude modulation for mu and beta phases where mu showed significant increase of amplitude for trough phase compared to peak phase ($p = 0.001$) and vice versa for mu phase ($p = 0.04$). The shaded area represents the 95% confidence interval.

We then investigated the effects of target phase and target rhythm on the late response. The late response did not show a significant main effect of phase; however, it showed a significant target phase × target oscillation interaction [$F(3, 57) = 5.66$, $p = 0.013$]. The late component showed an opposing phase dependent modulation for mu and beta rhythms. For mu-specific target, trough phase resulted in the increased modulation of the late response (1.03 n.u.) while peak phase resulted in the decreased modulation (0.97 n.u.). This modulation of the late response between the peak and trough phases was significantly different ($p = 0.001$). During beta-specific targeting, peak phase resulted in the increased response modulation (1.01 n.u.) while trough phase resulted in the decreased response modulation (Figure 3.2). Likewise, for beta-specific target, the modulation between peak and trough phases was statistically significant according to multiple comparisons ($p = 0.04$).

Overall, this showed higher phasic modulation of both early and late responses for mu-specific targeting compared to beta-specific targeting. Similarly, early responses showed larger changes compared to late responses. This underscores the roles of mu and beta phase on TMS evoked cortical responses at different latencies.

3.3.2. MEP and TEP Phase Relationship

Previously, we found that MEP excitability for mu and beta target oscillations have an opposing phase relationship at the group level. Wischnewski et al., 2022 showed mu-specific targeting results in high excitability for trough and rising phases. Conversely, beta-specific targeting results in high excitability for peak and fall in beta oscillations. Here, we calculated the preferred phase of the MEPs and TEP components for each participant to quantify the phase - excitability relationship. As expected, the distribution of the preferred phase was oriented towards trough and rising phases in mu and peak and fall phases in beta oscillations for MEPs. In the TEP analysis, the distribution of the preferred phase of the early TEP component was oriented towards falling and trough phases. For late TEP component, the orientation was dominant towards trough and rising phases (Figure 3.3A and Figure 3.4). This indicated that the early TEP component for mu target rhythm showed a 90^0 shift in the preferred phase relative to MEPs, whereas the late component showed the same phase preference as MEPs. However, neither the early nor late TEP component following beta specific stimulation showed a strong phase preference towards a particular orientation (Figure 3.3B and Figure 3.4).

3.3.3. Effect of Pre-TMS Power on Cortical Reponses

We ran two GLMMs for each target rhythm to study the effects of target phase and the pre-TMS band power on early and late components. For mu rhythm, we found significant main effects of phase (early component: $F = 69.37$, $p < 0.001$; late component: $F = 21.43$, $p < 0.001$) and pre-TMS mu power (early component: $F = 92.98$, $p < 0.001$; late component: $F = 25.54$, $p < 0.001$) and an interaction effect of phase × pre-TMS power (early component: $F = 41.00$, $p < 0.001$; late component: $F = 32.18$, $p < 0.001$) for both early and late TEP components. Interestingly, we only found a significant effect of pre-TMS beta power, but not phase, on the early and late TEP components when beta rhythm was targeted (early component: $F = 9.66$, $p = 0.002$; late component: $F = 11.77$, $p < 0.001$).

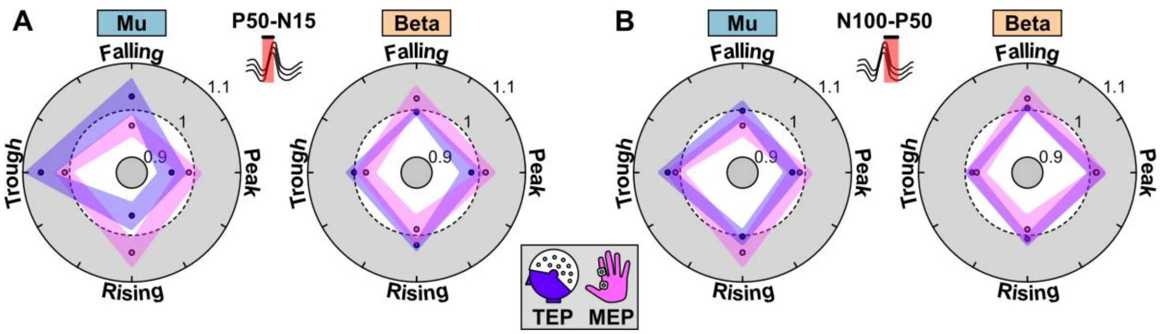

Figure 3.3 Relationship between corticospinal excitability and cortical responses. A) The comparison of relative changes of MEP and TEP amplitudes for the early component for mu and beta oscillations. B) The same comparison for the late component.

To study whether pre-TMS power is related to MEP amplitude and TEP amplitudes at the group level, we calculated the correlation between these measures. We found that the early and the late components during mu target rhythm were positively correlated with the pre-TMS power (early component: $r = 0.57$, $p = 0.008$ and late component: $r = 0.76$, $p < 0.001$) (Fig. 5A). For beta target rhythm, the early component showed a significant positive correlation with the pre-TMS beta power, but not the late component (early component: $r = 0.45$, $p = 0.048$ and late component: $r = 0.42$, $p = 0.067$) (Fig. 5). The strength of correlations suggests that pre-TMS mu power is the stronger determinant of the brain responses between the two dominant oscillations in the sensorimotor cortex.

We further studied the combined effects of pre-TMS mu and beta power on the early and late components by pooling the trials from all sessions and classifying the mu and beta power as ‘high’ and ‘low’ via a median split. Hence, the TEPs were divided into four classes: mu high - beta high, mu high - beta low, mu low -

beta high, mu low - beta low. The comparisons across groups indicate that both mu and beta power affected the early TEP component with increasing power resulting in increased TEP modulation (Fig. 5B). We performed Wilcoxon rank sum test to compare classes and found that they were pairwise significant (mu high-beta high vs. mu high-beta low: $z = 2.90$, $p = 0.004$, mu low-beta high vs. mu low-beta low: $z = 3.70$, $p < 0.001$). Interestingly, only the mu power and not the beta power showed an effect on the late component (Fig. 5B). The difference of late TEP modulation between mu high-beta high and mu high-beta low classes were not significant ($z = 0.60$, $p = 0.55$). Similarly, mu low-beta high and mu low-beta low groups did not show a significant difference ($z = 1.90$, $p = 0.06$). However, both classes with high mu power showed significantly higher modulation of late TEP component compared to both classes with low mu power irrespective of the beta power (mu high-beta high vs. mu low-beta high: $z = 3.70$, $p < 0.001$, mu high-beta high vs. mu low-beta low: $z = 3.58$, $p < 0.001$ and mu high-beta low vs. mu low-beta high: $z = 3.78$, $p < 0.001$, mu high-beta low vs. mu low-beta low: $z = 3.66$, $p < 0.001$). In order to verify that the power of other frequency bands (delta and theta) do not contribute to TEP modulation, we classified TEPs into high and low power states of these bands. However, the results did not indicate significant modulation of TEP amplitudes for early or late components in both delta and theta bands. Hence, the results indicate that early response is driven by a combination of mu and beta power whereas the late component is driven by mu power alone.

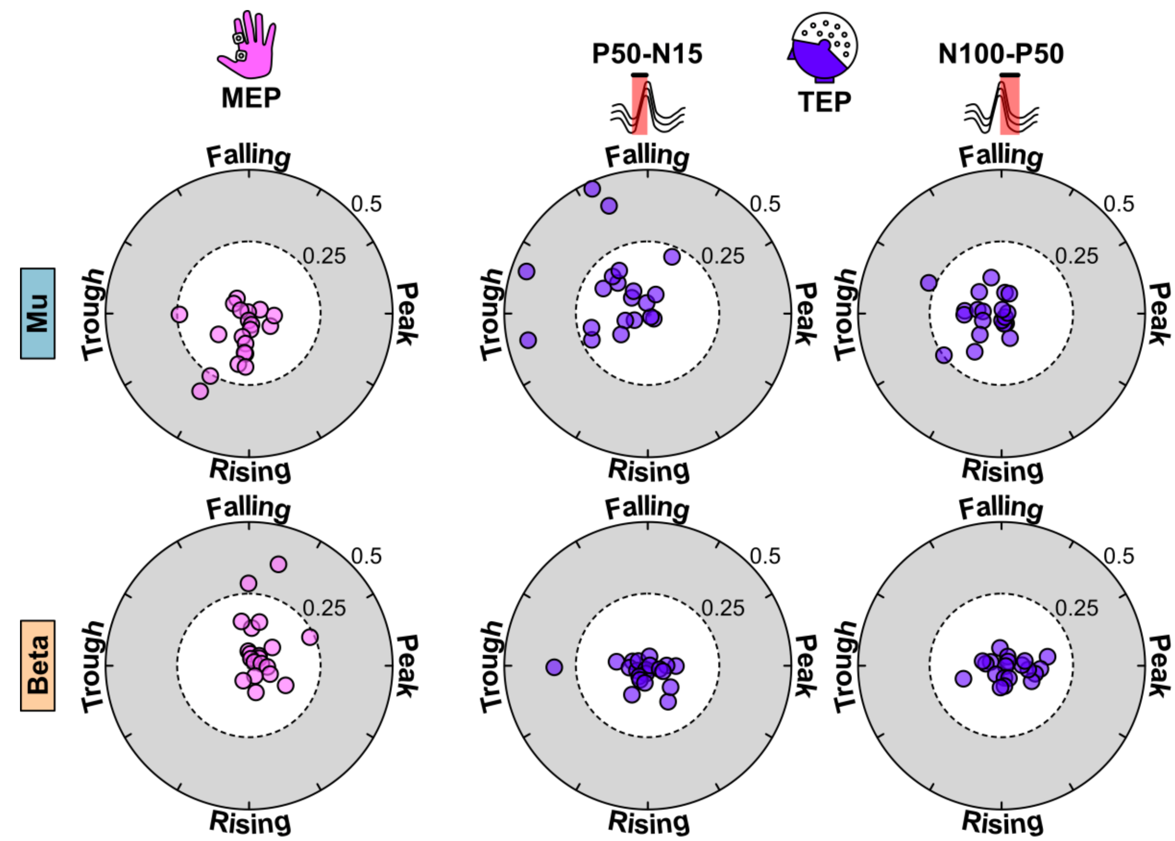

Figure 3.4 Individual phase preferences of MEP and TEP components. (Top) MEPs generated during mu target rhythm have a phase preference of rising and trough phases while the early TEP component is preferentially modulated by falling and trough phases. The late component shows a phase preference similar to that of MEPs where the preferred orientation is towards trough and rising phases. (Bottom) MEPs generated when phases of beta rhythm were targeted, are preferentially modulated by falling and peak phases (opposite to mu). Neither the early component nor the late component showed a preferential modulation of TEP amplitude to a specific phase.

3.4. Discussion

In this study, we investigated the effects of state-dependent stimulation of the motor cortex on cortical responses for mu and beta oscillations and their relationship to corticospinal excitability. We defined an immediate oscillatory state as phase and power of oscillation of interest. The oscillatory phase was extracted in real-time for ad hoc stimulation, while pre-TMS band power was estimated in a post-hoc manner. First, we found that the early cortical responses (<50 ms) were modulated by mu and beta phase during the TMS pulse. The later component (50-100 ms) also showed modulation of cortical responses, albeit to a lesser degree. Overall, mu-specific targeting elicited larger changes in amplitudes compared to beta. Second, we found that the M1-muscle excitability measured through MEPs showed a different phase preference to that of the early cortical response in mu-specific targeting. For the same target rhythm, the phase preference between later cortical activation and MEPs was similar. Finally, we found that pre-TMS mu and beta power affect early cortical responses independent of each other. However, only pre-TMS mu power affects the later cortical response.

Previous studies have found that N15 is indicative of early excitation of motor and premotor areas (Esser et al., 2006; Litvak et al., 2007; Mäki & Ilmoniemi, 2010), P50 reflects the reafferent signals from the stimulated muscle (motor-basal ganglia cortical loop) (Desideri et al., 2019; Mäki & Ilmoniemi, 2010; Petrichella et al., 2017), and N100 is related to GABAergic inhibition and cortical silent period (Bonnard et al., 2009; Farzan et al., 2013; V. V. Nikulin, Kicic, et al., 2003; Premoli et al., 2014; Rogasch et al., 2013; Rogasch & Fitzgerald, 2013b). In addition to these components, P30 and N45 are reported (Bertazzoli et al., 2021; Rogasch et al., 2022). However, individual variability exists pertaining to these components. In our study, several participants revealed the P30-N45-P60 complex (we denote the second positive peak in this complex as P50 considering the group level latency).

This individual variability meant that it was not a reliable measure at the group level. Consequently, the global response did not delineate P30 and N45 components, thus we constrained our analysis to P50 component. Our study shows that the strength of early cortical excitation and muscle reafferent signal, as estimated by P50-N15 component, is highly modulated by the phase of the mu oscillation. We observed that trough and falling phases of the mu oscillation caused increased modulation of this response. Targeting beta oscillation modulated this to a lesser degree, with rising phase showing increased activity. However, the physiological processes associated with the late components showed opposing effects for mu and beta rhythms. We also found that the early component was more affected by phase targeting compared to the late component. This implies that the phase affected early activation which correlates to MEP generation more than the later components. The strong modulation of early component by mu phase thus indicates that mu rhythm is a driving factor of local brain excitability. The contribution of beta rhythm to this modulation is weaker according to our results. The observation that the overall relative changes of the TEP components were greater for mu compared to beta oscillations could also corroborate the importance of mu rhythm in cortical response generation.

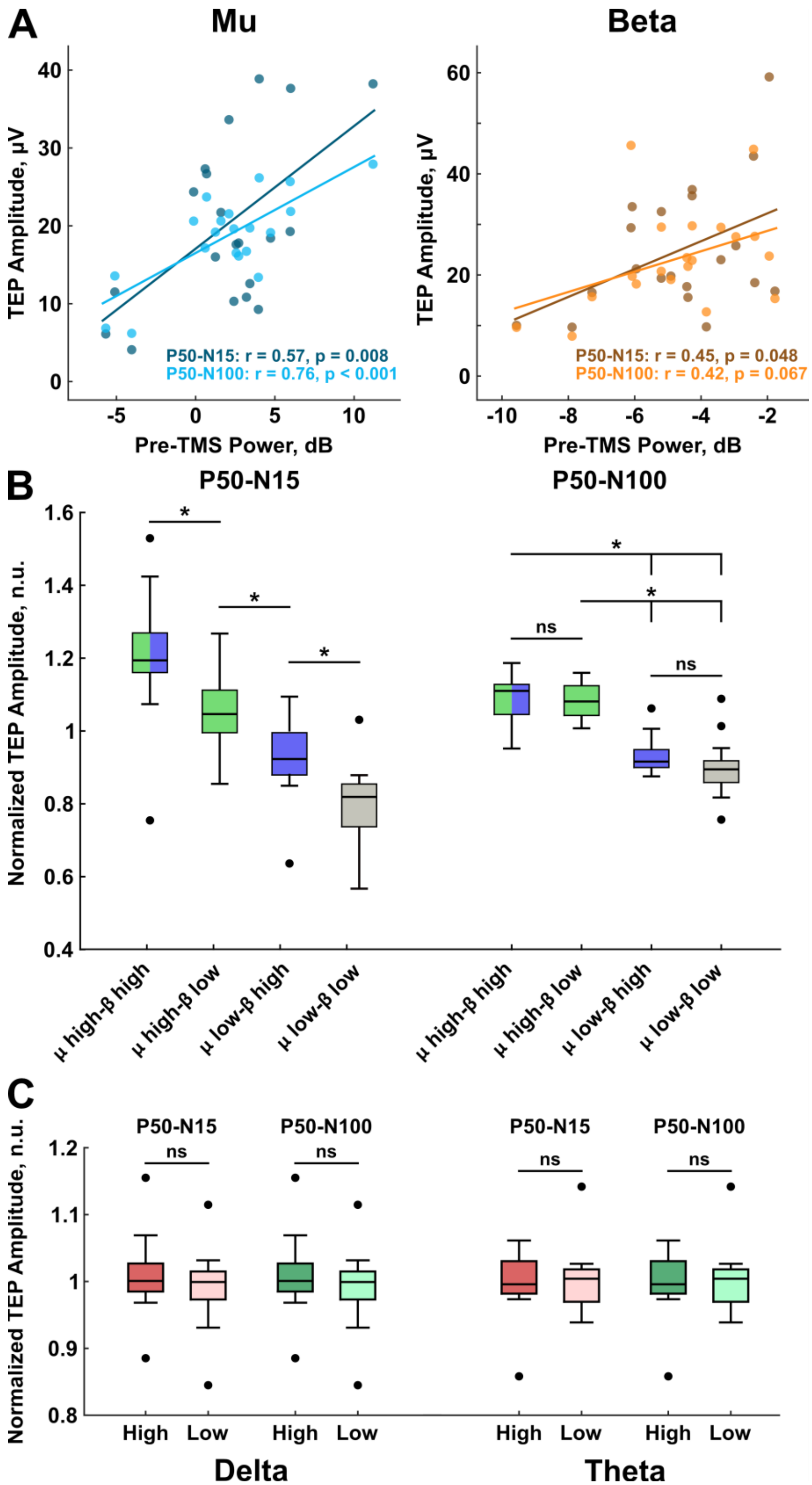

A
Mu
Beta
TEP Amplitude, μV
Pre-TMS Power, dB
P50-N15: r = 0.57, p = 0.008
P50-N100: r = 0.76, p < 0.001
P50-N15: r = 0.45, p = 0.048
P50-N100: r = 0.42, p = 0.067
B
P50-N15
P50-N100
Normalized TEP Amplitude, n.u.
μ high-β high
μ high-β low
μ low-β high
μ low-β low
ns
C
Normalized TEP Amplitude, n.u.
High
Low
Delta
Theta

Figure 3.5 The effects of pre-TMS power on TEP components. A) The group level correlation between pre-TMS power and TEP components. Pre-TMS mu (8-13 Hz) band power showed a strong correlation with both early ($r = 0.57$, $p = 0.008$) and late ($r = 0.76$, $p < 0.001$) TEP components (left). Pre-TMS beta (14-30 Hz) bad power showed a moderate correlation with the early TEP component ($r = 0.45$, $p = 0.048$); however, the correlation was not significant for the late component ($r = 0.42$, $p = 0.067$). Each dot in the scatter plot represents the average power and average TEP amplitude across the four phases per participant. B) The combined effect of pre-TMS mu and beta power on the TEP components. The early component showed highest modulation when both mu and beta power were high and lowest modulation when both mu and beta power were low. High mu-low beta and low mu-high beta resulted in higher than average and lower than average modulation respectively. Wilcoxon rank sum tests showed that the relative changes of TEP amplitudes in these groups were significantly different (left). The modulation of late component was not affected by beta power. Regardless of beta power, high mu power resulted in higher TEP modulation and low mu power resulted in lower TEP modulation. Significant differences were not observed within groups with high mu power or low mu power. However, differences were significant across groups with high mu power and low mu power (right). C) The power of other bands of interest, delta and theta, did not contribute to modulation of both early and late components. Outliers are marked in black circles. * $p < 0.05$, n.s. = not significant.

A key finding in this study is that the modulation of early cortical response (as measured by TEPs) does not resemble the same pattern as the M1-muscle excitability for mu-specific target (as measured by MEPs). Instead, the early direct cortical activation and the muscle excitability show a different phase preference that is 90^0 out of phase to each other. This could be explained by the cortical origins of early TEP components and MEPs. Sensor-level and source level analysis of TEP components have shown widespread activity in M1, supplementary motor area, and superior parietal lobule during the early response (Litvak et al., 2007; Zazio et al., 2021). On the other hand, MEPs from FDI muscle have been shown to be generated by gyral crown and upper parts of the sulcal wall in M1 (Salvador et al., 2011; Weise et al., 2020). Essentially, early response captured by C3 represents the aggregate activity from a wider cortical area. In contrast, the MEPs represent the activity of a small subset of neurons that have a specific orientation. Hence, we could expect this subset of neurons to be modulated by a phase of ongoing oscillation that is different from overall population activated by TMS. Interestingly, the preferred phase of both later cortical response and M1-muscle excitability was oriented towards trough and rising phases in mu-specific targeting. As previously discussed, the late components reflect the reafferent information from the motor-basal ganglia-cortical loop (P50) and cortical inhibition and cortical silent period (N100). Given that trough and rising phases indicate a high M1-excitability state, the feedback mechanisms may lead to increased inhibition (Fecchio et al., 2017; Roos et al., 2021). This would result in increased late response for the same phases. Therefore, the early response is likely related to TMS pulse itself, whereas the late components are an after effect of MEP generation. We did not find an alignment of the preferred phases for beta rhythm. This suggested an influence of beta phase on corticospinal excitability and cortical responses that was difficult to reconcile.

We further analyzed whether pre-TMS band power explains the variability of the TEP amplitudes at the trial and the group level. At trial level, both pre-TMS mu power and the target phase of mu oscillation affected brain responses. However, when targeting beta oscillations, only pre-TMS beta power had an effect on brain responses. In our previous study, Wischnewski et al. showed that both phase and pre-TMS mu power (when mu oscillations were targeted) play a role in corticospinal excitability as measured by MEPs. For beta-specific targeting, only phase determined corticospinal excitability. Thus, there is general agreement of the effect pre-TMS mu power and phase on MEPs and TEPs. At the group level, the relationship between pre-TMS band power and TEP components showed a positive association for mu rhythm, confirming the trial level observation. For beta, the early component showed a significant positive association with pre-TMS beta power, but not the later component. We sought to explain the combined effect of pre-TMS mu and beta power on all TEP responses by classifying them into high and low power states. Accordingly, the post-hoc analysis we performed showed that early component is modulated by the power of both mu and beta oscillations. However, only pre-TMS mu power significantly modulated the late component, shedding light on distinct roles of mu and beta in cortical response generation. This confirms the predominant role played by sensorimotor mu oscillatory characteristics in early local excitability and late cortical responses. However, the role of sensorimotor beta characteristics, especially in later cortical responses is unclear. It has been shown that sensorimotor mu oscillations are related to GABA inhibitory activity (Bergmann et al., 2019) and inversely related to blood oxygen level dependent (BOLD) signal in the cortical-subcortical motor network (Peters et al., 2020). This could explain the positive association between the late component, which is a marker of cortical inhibition and pre-TMS mu power. The effect of both phase and power on corticospinal excitability for sensorimotor mu oscillations has been explored previously for peak and trough phases, which supports the main and interaction effects revealed by the GLMMs (Ozdemir et al., 2022). In contrast, the role of sensorimotor beta in the motor cortex is not fully understood. Studies have shown that beta power is associated with voluntary and task related motor activity (Jana et al., 2020; Kilavik et al., 2013) and that resting beta power does not affect the propagation of TMS excitations in the motor cortex (Peters et al., 2020). In fact, movement related beta decrease has been shown during spontaneous and trigger movement (Kilavik et al., 2013) whereas inhibition of movement leads to higher beta power (Jana et al., 2020; Swann et al., 2012; Wagner et al., 2018). The fact that the participants in our study did not perform voluntary muscle contractions or motor tasks could explain weaker correlation between the cortical responses and pre-TMS beta power compared to pre-TMS mu power.

It is not fully established if TMS-evoked cortical responses are generated by oscillatory phase-resetting or by adding to the ongoing oscillation. Thus, one could consider if our brain state-dependent TEP results are confounded by pre-TMS voltage differences. Some studies have suggested phase-resetting of ongoing oscillations by TMS or other forms of stimulus presentation (Gruber et al., 2005; Hanslmayr et al., 2007; Kawasaki et al., 2014; Paus et al., 2001). However, other studies have found evidence against this that phase is preserved following TMS up to 200 ms through measures of phase preservation index (PPI) (Desideri et al., 2019; Mazaheri & Jensen, 2006). To clarify this question, we first calculated the phase preservation index for C3 and surrounding electrodes for real TMS trials and non-stimulated trials, but we were not able to find evidence for phase preservation (Supplementary Fig. 1). Thus, we measured early and later components as a difference between two consecutive TEP peaks (P50-N15 and N100-P50) (Bergmann et al., 2012; Desideri et al., 2019; Kruglikov & Schiff, 2003). The use of peak-to-peak values mitigates possible confounds of phase preservation or phase resetting.

Here, we only used phase of oscillation as an experimentally controlled variable, while pre-TMS power was estimated post hoc. Studies have shown the importance of power of oscillation to elicit high and low excitability states (Ozdemir et al., 2022). In the future, experimental studies may consider delivering TMS based on the combined pre-defined phase and power definitions. It should be noted that we removed the first 15 ms after TMS pulse from the analysis due to TMS pulse artifact. This is a standard approach; however, very early evoked activity around 1-2 ms after TMS delivery is thus not captured by our analysis. Specific experimental settings showed that very early responses may represent activation of pyramidal tract neurons and corticospinal neurons directly and via monosynaptic connections (Di Lazzaro et al., 1998).

The present results characterize brain state dependency of motor cortex. An exciting future direction is to extend this work to other brain areas. Furthermore, real-time closed-loop stimulation systems could be developed by taking more state variables, such as band power and network connectivity, into account.

Chapter 4: Conclusions and Perspectives

4.1. Conclusions

In Chapter 1 of this dissertation, I introduced transcranial magnetic stimulation (TMS) and its significance as both a research tool and a therapeutic intervention. I also discussed some of the gaps in knowledge related to the mechanisms of TMS action and the relationship between electrophysiological biomarkers and physiological outcomes. I then explored the suitability of non-human primate models for understanding these mechanisms. Specifically, I sought to address the following questions related to TMS:

- What is the effect of TMS parameters (i.e., dose and coil location) on electrophysiological biomarkers?
- How can we separate peripheral (i.e., auditory and somatosensory) responses from central TMS effects?
- How does phase-dependent TMS stimulation of the motor cortex affect cortical responses?
- Is there a well-defined relationship between the phase preference of corticospinal excitability and cortical responses?

- What is the relationship between the power of motor cortical oscillations and cortical responses?

In the subsequent chapters, I discuss in detail how I addressed these issues through experimental research in non-human primates and humans.

In Chapter 2, I studied the effects of TMS on the non-human primate brain using invasive electrophysiology. This approach overcomes the limitations of spatial resolution associated with TMS-EEG in humans and serves as a translational model. We designed experiments to advance our understanding of TMS dose dependency and the effects of stimulation location on local field potentials, quantifying them using electrophysiological biomarkers. We identified a sigmoidal relationship between TMS intensity and the TEP component N50, an electrophysiological biomarker of TMS activation. We also investigated how this component was modulated by coil location and how the coil-to-contact distance affected its magnitude. Additionally, we controlled for peripheral auditory and somatosensory stimulation and compared changes in the cortical response, allowing us to dissociate centrally induced TMS effects from peripheral effects. These findings are critical for understanding biomarkers of TMS effects, which could be beneficial for therapeutic applications.

In Chapter 3, I investigated mechanisms of phase-dependent brain stimulation in the human motor cortex using TMS-EEG. I utilized a dataset acquired by targeting four phases of mu and beta oscillations in the motor cortex. I quantified cortical responses in terms of N15, P50, and N100 components and studied how these components were modulated by the phase of ongoing oscillations. We identified specific phases of oscillations that showed higher and lower modulation of cortical responses for each frequency band. We then examined whether the phasic relationship of cortical responses is similar to that of cortical excitability, quantifying this by calculating the preferred phase of cortical responses and corticospinal excitability. We identified a distinct phase preference relationship between cortical excitability and cortical responses for mu-specific stimulation, but this was not evident for beta-specific stimulation, highlighting the dominant role of mu phase in the motor cortex. Finally, I investigated the role of the power of ongoing oscillations in cortical response generation. We found that early cortical responses were affected by both pre-TMS mu and beta oscillations, showing an interaction effect of both frequency bands. However, the late component was only modulated by pre-TMS mu oscillations, underscoring the distinct roles of mu and beta oscillations in underlying physiological mechanisms reflected in TEP cortical responses.

Overall, this dissertation aims to understand the electrophysiological biomarkers associated with TMS in non-human primates and humans and how they can be utilized to elucidate the underlying mechanisms of TMS. I present experiments, along with EEG/sEEG data analysis pipelines, statistical analyses, and physiological interpretations of these results, to better explain these mechanisms.

4.2. Perspectives

In this section, we discuss the limitations of the current studies and how future work can improve upon the findings presented here.

In the non-human primate study, we investigated electrophysiological biomarkers in anesthetized monkeys during TMS. While cortical responses in the anesthetized state provide insights into the mechanisms of TMS action, the brain state of awake, behaving monkeys is more complex and provides a deeper understanding of how TMS interacts with the brain's behavioral states. Thus, conducting these experiments in awake, behaving monkeys would allow us to study the effects of TMS on a behavioral level. In our study, the biomarker of activation (N50) showed an inverse relationship with the coil-to-contact distance. However, we did not find a modulatory effect with the movement of the coil; in some stimulation locations, contacts away from the coil showed a high response. To investigate this further, functional connectivity across different brain regions needs to be assessed using fMRI or diffusion tractography. Finally, the relationship between invasive electrophysiological biomarkers and EEG biomarkers needs to be established in non-human primates through concurrent TMS, iEEG, and EEG experiments. This is critical for translating these results to human TMS-EEG studies.

In the phase-dependent TMS study, we sought to understand how biomarkers are modulated by the phase of oscillations, i.e., brain state. In the current study, we estimated the brain state through the phase of oscillation. However, it has been shown that oscillatory power also plays a role in brain state. We analyzed this by post-hoc extraction of power. Further development of closed-loop systems that account for oscillatory power would allow us to investigate this more conveniently. We studied the relationship between MEPs and cortical responses by calculating the preferred phase of each measurement. We explained this relationship through the cytoarchitecture of the brain responsible for the generation of MEPs and cortical responses. A future application would be to validate these findings using a computational neuron model of the motor cortex. While our study is confined to the motor cortex, where a measure of behavioral outcome is readily available, it would be interesting to apply the concept of state-dependent stimulation to other clinically relevant brain regions, such as the prefrontal cortex. This would allow us to study the relationship between disease states and biomarkers, and subsequently apply state-dependent brain stimulation to optimize treatment outcomes and track objective markers of disease states.

Bibliography

Alekseichuk, I., Mantell, K., Shirinpour, S., & Opitz, A. (2019). Comparative modeling of transcranial magnetic and electric stimulation in mouse, monkey, and human. *NeuroImage*, *194*(February), 136–148. https://doi.org/10.1016/j.neuroimage.2019.03.044

Allison, T., Mccarthy, G., Wood, C. C., & Jones, S. J. (1991). Potentials evoked in human and monkey cerebral cortex by stimulation of the median nerve: A review of scalp and intracranial recordings. *Brain*, *114*(6), 2465–2503. https://doi.org/10.1093/brain/114.6.2465

Barker, A. T., Jalinous, R., & Freeston, I. L. (1985). Non-invasive magnetic stimulation of human motor cortex. *Lancet (London, England)*, *1*(8437), 1106–1107. https://doi.org/10.1016/s0140-6736(85)92413-4

Bell, A. J., & Sejnowski, T. J. (1995). An information-maximization approach to blind separation and blind deconvolution. *Neural Computation*, *7*(6), 1129–1159. https://doi.org/10.1162/neco.1995.7.6.1129

Berger, B., Minarik, T., Liuzzi, G., Hummel, F. C., & Sauseng, P. (2014). EEG Oscillatory Phase-Dependent Markers of Corticospinal Excitability in the Resting Brain. *BioMed Research International*, *2014*, 936096. https://doi.org/10.1155/2014/936096

Bergmann, T. O., Lieb, A., Zrenner, C., & Ziemann, U. (2019). Pulsed Facilitation of Corticospinal Excitability by the Sensorimotor μ-Alpha Rhythm. *The Journal of Neuroscience*, *39*(50), 10034. https://doi.org/10.1523/JNEUROSCI.1730-19.2019

Bergmann, T. O., Mölle, M., Schmidt, M. A., Lindner, C., Marshall, L., Born, J., & Siebner, H. R. (2012). EEG-Guided Transcranial Magnetic Stimulation Reveals Rapid Shifts in Motor Cortical Excitability during the Human Sleep Slow Oscillation. *Journal of Neuroscience*, *32*(1), 243–253. https://doi.org/10.1523/JNEUROSCI.4792-11.2012

Bertazzoli, G., Esposito, R., Mutanen, T. P., Ferrari, C., Ilmoniemi, R. J., Miniussi, C., & Bortoletto, M. (2021). The impact of artifact removal approaches on TMS–EEG signal. *NeuroImage*, *239*, 118272. https://doi.org/10.1016/j.neuroimage.2021.118272

Bikmullina, R., Kičić, D., Carlson, S., & Nikulin, V. V. (2009). Electrophysiological correlates of short-latency afferent inhibition: A combined EEG and TMS study. *Experimental Brain Research*, *194*(4), 517–526. https://doi.org/10.1007/s00221-009-1723-7

Bonato, C., Miniussi, C., & Rossini, P. M. (2006). Transcranial magnetic stimulation and cortical evoked potentials: A TMS/EEG co-registration study. *Clinical Neurophysiology*, *117*(8), 1699–1707. https://doi.org/10.1016/j.clinph.2006.05.006

Bonnard, M., Spieser, L., Meziane, H. B., De Graaf, J. B., & Pailhous, J. (2009). Prior intention can locally tune inhibitory processes in the primary motor cortex: Direct evidence from combined TMS-EEG. *European Journal of Neuroscience*, *30*(5), 913–923. https://doi.org/10.1111/j.1460-9568.2009.06864.x

Brasil-Neto, J. P., Pascual-Leone, A., Valls-Sole, J., Cohen, L. G., & Hallett, M. (1992). Focal transcranial magnetic stimulation and response bias in a forced-choice task. *Journal of Neurology, Neurosurgery & Psychiatry*, *55*(10), 964–966. https://doi.org/10.1136/jnnp.55.10.964

Brasso, C., Cisotto, M., Del Favero, E., Giordano, B., Villari, V., & Rocca, P. (2023). Impact of COVID-19 pandemic on major depressive disorder in acute psychiatric inpatients. *Frontiers in Psychology*, *14*, 1181832. https://doi.org/10.3389/fpsyg.2023.1181832

Brunoni, A. R., Chaimani, A., Moffa, A. H., Razza, L. B., Gattaz, W. F., Daskalakis, Z. J., & Carvalho, A. F. (2017). Repetitive transcranial magnetic stimulation for the acute treatment of major depressive episodes a systematic review with network meta-analysis. *JAMA Psychiatry*, *74*(2), 143–152. https://doi.org/10.1001/jamapsychiatry.2016.3644

Buzsáki, G., Anastassiou, C. A., & Koch, C. (2012). The origin of extracellular fields and currents—EEG, ECoG, LFP and spikes. *Nature Reviews Neuroscience*, *13*(6), 407–420. https://doi.org/10.1038/nrn3241

Casula, E. P., Tarantino, V., Basso, D., Arcara, G., Marino, G., Toffolo, G. M., Rothwell, J. C., & Bisiacchi, P. S. (2014). Low-frequency rTMS inhibitory effects in the primary motor cortex: Insights from TMS-evoked potentials. *NeuroImage*, *98*, 225–232. https://doi.org/10.1016/j.neuroimage.2014.04.065

Combrisson, E., Perrone-Bertolotti, M., Soto, J. L., Alamian, G., Kahane, P., Lachaux, J.-P., Guillot, A., & Jerbi, K. (2017). From intentions to actions: Neural oscillations encode motor processes through phase, amplitude and phase-amplitude coupling. *NeuroImage*, *147*, 473–487. https://doi.org/10.1016/j.neuroimage.2016.11.042

Conde, V., Tomasevic, L., Akopian, I., Stanek, K., Saturnino, G. B., Thielscher, A., Bergmann, T. O., & Siebner, H. R. (2019). The non-transcranial TMS-evoked potential is an inherent source of ambiguity in TMS-EEG studies. *NeuroImage*, *185*(June 2018), 300–312. https://doi.org/10.1016/j.neuroimage.2018.10.052

Darling, W. G., Wolf, S. L., & Butler, A. J. (2006). Variability of motor potentials evoked by transcranial magnetic stimulation depends on muscle activation. *Experimental Brain Research*, *174*(2), 376–385. https://doi.org/10.1007/s00221-006-0468-9

Daskalakis, Z. J., Farzan, F., Barr, M. S., Maller, J. J., Chen, R., & Fitzgerald, P. B. (2008). Long-Interval Cortical Inhibition from the Dorsolateral Prefrontal Cortex: A TMS–EEG Study. *Neuropsychopharmacology*, *33*(12), 2860–2869. https://doi.org/10.1038/npp.2008.22

Denslow, S., Lomarev, M., George, M. S., & Bohning, D. E. (2005). Cortical and subcortical brain effects of Transcranial Magnetic Stimulation (TMS)-induced movement: An interleaved TMS/functional magnetic resonance imaging study. *Biological Psychiatry*, *57*(7), 752–760. https://doi.org/10.1016/j.biopsych.2004.12.017

Desideri, D., Zrenner, C., Ziemann, U., & Belardinelli, P. (2019). Phase of sensorimotor μ-oscillation modulates cortical responses to transcranial magnetic stimulation of the human motor cortex. *The Journal of Physiology*, *597*(23), 5671–5686. https://doi.org/10.1113/JP278638

Di Lazzaro, V., Oliviero, A., Profice, P., Saturno, E., Pilato, F., Insola, A., Mazzone, P., Tonali, P., & Rothwell, J. C. (1998). Comparison of descending volleys evoked by transcranial magnetic and electric stimulation in conscious humans. *Electroencephalography and Clinical Neurophysiology*, *109*(5), 397–401. https://doi.org/10.1016/s0924-980x(98)00038-1

Esser, S. K., Huber, R., Massimini, M., Peterson, M. J., Ferrarelli, F., & Tononi, G. (2006). A direct demonstration of cortical LTP in humans: A combined TMS/EEG study. *Brain Research Bulletin*, *69*(1), 86–94. https://doi.org/10.1016/j.brainresbull.2005.11.003

Fair, D. A., Miranda-Dominguez, O., Snyder, A. Z., Perrone, A., Earl, E. A., Van, A. N., Koller, J. M., Feczko, E., Tisdall, M. D., van der Kouwe, A., Klein, R. L., Mirro, A. E., Hampton, J. M., Adeyemo, B., Laumann, T. O., Gratton, C., Greene, D. J., Schlaggar, B. L., Hagler, D. J., … Dosenbach, N. U. F. (2020). Correction of respiratory artifacts in MRI head motion estimates. *NeuroImage*, *208*(October 2019), 116400. https://doi.org/10.1016/j.neuroimage.2019.116400

Farzan, F., Barr, M. S., Hoppenbrouwers, S. S., Fitzgerald, P. B., Chen, R., Pascual-Leone, A., & Daskalakis, Z. J. (2013). The EEG correlates of the TMS-induced EMG silent period in humans. *NeuroImage*, *83*, 120–134. https://doi.org/10.1016/j.neuroimage.2013.06.059

Fecchio, M., Pigorini, A., Comanducci, A., Sarasso, S., Casarotto, S., Premoli, I., Derchi, C.-C., Mazza, A., Russo, S., Resta, F., Ferrarelli, F., Mariotti, M., Ziemann, U., Massimini, M., & Rosanova, M. (2017). The spectral features of EEG responses to transcranial magnetic stimulation of the primary motor cortex depend on the amplitude of the motor evoked potentials. *PLOS ONE*, *12*(9), e0184910. https://doi.org/10.1371/journal.pone.0184910

Ferrarelli, F., Massimini, M., Sarasso, S., Casali, A., Riedner, B. A., Angelini, G., Tononi, G., & Pearce, R. A. (2010). Breakdown in cortical effective connectivity during midazolam-induced loss of consciousness. *Proceedings of the National Academy of Sciences of the United States of America*, *107*(6), 2681–2686. https://doi.org/10.1073/pnas.0913008107

Fox, M. D., Halko, M. A., Eldaief, M. C., & Pascual-Leone, A. (2012). Measuring and manipulating brain connectivity with resting state functional connectivity magnetic resonance imaging (fcMRI) and transcranial magnetic stimulation (TMS). *NeuroImage*, *62*(4), 2232–2243. https://doi.org/10.1016/j.neuroimage.2012.03.035

Gersner, R., Kravetz, E., Feil, J., Pell, G., & Zangen, A. (2011). Long-term effects of repetitive transcranial magnetic stimulation on markers for neuroplasticity: Differential outcomes in anesthetized and awake animals. *The Journal of Neuroscience : The Official Journal of the Society for Neuroscience*, *31*(20), 7521–7526. https://doi.org/10.1523/JNEUROSCI.6751-10.2011

Goto, T., Nakata, Y., Saito, H., Ishiguro, Y., Niimi, Y., & Morita, S. (2001). The midlatency auditory evoked potentials predict responsiveness to verbal commands in patients emerging from anesthesia with xenon, isoflurane, and sevoflurane but not with nitrous oxide. *Anesthesiology*, *94*(5), 782–789. https://doi.org/10.1097/00000542-200105000-00015

Greenberg, P., Chitnis, A., Louie, D., Suthoff, E., Chen, S.-Y., Maitland, J., Gagnon-Sanschagrin, P., Fournier, A.-A., & Kessler, R. C. (2023). The Economic Burden of Adults with Major Depressive Disorder in the United States (2019). *Advances in Therapy*, *40*(10), 4460–4479. https://doi.org/10.1007/s12325-023-02622-x

Greve, D. N., & Fischl, B. (2009). Accurate and robust brain image alignment using boundary-based registration. *NeuroImage*, *48*(1), 63–72. https://doi.org/10.1016/j.neuroimage.2009.06.060

Grider, M. H., Belcea, C. Q., Covington, B. P., Reddy, V., & Sharma, S. (2024). Neuroanatomy, Nodes of Ranvier. In *StatPearls*. StatPearls Publishing.

Groppa, S., Oliviero, A., Eisen, A., Quartarone, A., Cohen, L. G., Mall, V., Kaelin-Lang, A., Mima, T., Rossi, S., Thickbroom, G. W., Rossini, P. M., Ziemann, U., Valls-Solé, J., & Siebner, H. R. (2012). A practical guide to diagnostic transcranial magnetic stimulation: Report of an IFCN committee. *Clinical Neurophysiology : Official Journal of the International Federation of Clinical Neurophysiology*, *123*(5), 858–882. https://doi.org/10.1016/j.clinph.2012.01.010

Gruber, W. R., Klimesch, W., Sauseng, P., & Doppelmayr, M. (2005). Alpha Phase Synchronization Predicts P1 and N1 Latency and Amplitude Size. *Cerebral Cortex*, *15*(4), 371–377. https://doi.org/10.1093/cercor/bhh139

Hallett, M. (2007). Transcranial magnetic stimulation: A primer. *Neuron*, *55*(2), 187–199. https://doi.org/10.1016/j.neuron.2007.06.026

Hanslmayr, S., Klimesch, W., Sauseng, P., Gruber, W., Doppelmayr, M., Freunberger, R., Pecherstorfer, T., & Birbaumer, N. (2007). Alpha Phase Reset Contributes to the Generation of ERPs. *Cerebral Cortex*, *17*(1), 1–8. https://doi.org/10.1093/cercor/bhj129

Hayashi, T., Ohnishi, T., Okabe, S., Teramoto, N., Nonaka, Y., Watabe, H., Imabayashi, E., Ohta, Y., Jino, H., Ejima, N., Sawada, T., Iida, H., Matsuda, H., & Ugawa, Y. (2004). Long-term effect of motor cortical repetitive transcranial magnetic stimulation induces. *Annals of Neurology*, *56*(1), 77–85. https://doi.org/10.1002/ana.20151

Herrmann, L. L., Hons, M. A., & Ebmeier, K. P. (2006). *Factors Modifying the Efficacy of Transcranial Magnetic*. 1870–1876.

Hoogendam, J. M., Ramakers, G. M. J., & Di Lazzaro, V. (2010). Physiology of repetitive transcranial magnetic stimulation of the human brain. *Brain Stimulation*, *3*(2), 95–118. https://doi.org/10.1016/j.brs.2009.10.005

Horvath, J. C., Perez, J. M., Forrow, L., Fregni, F., & Pascual-Leone, A. (2011). Transcranial magnetic stimulation: A historical evaluation and future prognosis of therapeutically relevant ethical concerns. *Journal of Medical Ethics*, *37*(3), 137–143. https://doi.org/10.1136/jme.2010.039966

Huang, Y.-Z., Edwards, M. J., Rounis, E., Bhatia, K. P., & Rothwell, J. C. (2005). Theta Burst Stimulation of the Human Motor Cortex. *Neuron*, *45*(2), 201–206. https://doi.org/10.1016/j.neuron.2004.12.033

Ilmoniemi, R. J., & Kičić, D. (2010). Methodology for Combined TMS and EEG. *Brain Topography*, *22*(4), 233–248. https://doi.org/10.1007/s10548-009-0123-4

Ilmoniemi, R. J., Virtanen, J., Ruohonen, J., Karhu, J., Aronen, H. J., Näätänen, R., & Katila, T. (1997). Neuronal responses to magnetic stimulation reveal cortical reactivity and connectivity: *NeuroReport*, *8*(16), 3537–3540. https://doi.org/10.1097/00001756-199711100-00024

Jana, S., Hannah, R., Muralidharan, V., & Aron, A. R. (2020). Temporal cascade of frontal, motor and muscle processes underlying human action-stopping. *eLife*, *9*, e50371. https://doi.org/10.7554/eLife.50371

Jannati, A., Oberman, L. M., Rotenberg, A., & Pascual-Leone, A. (2023). Assessing the mechanisms of brain plasticity by transcranial magnetic stimulation. *Neuropsychopharmacology*, *48*(1), 191–208. https://doi.org/10.1038/s41386-022-01453-8

Jenkinson, M., Bannister, P., Brady, M., & Smith, S. (2002). Improved Optimization for the Robust and Accurate Linear Registration and Motion Correction of Brain Images. *NeuroImage*, *17*(2), 825–841. https://doi.org/10.1006/nimg.2002.1132

Jenkinson, M., & Smith, S. (2001). A global optimisation method for robust affine registration of brain images. *Medical Image Analysis*, *5*(2), 143–156. https://doi.org/10.1016/S1361-8415(01)00036-6

Kadosh, R. C., & Elliott, P. (2013). Brain stimulation has a long history. *Nature*, *500*(7464), 529–529. https://doi.org/10.1038/500529d

Kähkönen, S., Komssi, S., Wilenius, J., & Ilmoniemi, R. J. (2005). Prefrontal transcranial magnetic stimulation produces intensity-dependent EEG responses in humans. *NeuroImage*, *24*(4), 955–960. https://doi.org/10.1016/j.neuroimage.2004.09.048

Kähkönen, S., Wilenius, J., Komssi, S., & Ilmoniemi, R. J. (2004). Distinct differences in cortical reactivity of motor and prefrontal cortices to magnetic stimulation. *Clinical Neurophysiology*, *115*(3), 583–588. https://doi.org/10.1016/j.clinph.2003.10.032

Karabanov, A. N., Madsen, K. H., Krohne, L. G., & Siebner, H. R. (2021). Does pericentral mu-rhythm “power” corticomotor excitability? – A matter of EEG perspective. *Brain Stimulation*, *14*(3), 713–722. https://doi.org/10.1016/j.brs.2021.03.017

Kawasaki, M., Uno, Y., Mori, J., Kobata, K., & Kitajo, K. (2014). Transcranial magnetic stimulation-induced global propagation of transient phase resetting associated with directional information flow. *Frontiers in Human Neuroscience*, *8*. https://doi.org/10.3389/fnhum.2014.00173

Kerwin, L. J., Keller, C. J., Wu, W., Narayan, M., & Etkin, A. (2018). Test-retest reliability of transcranial magnetic stimulation EEG evoked potentials. *Brain Stimulation*, *11*(3), 536–544. https://doi.org/10.1016/j.brs.2017.12.010

Kičić, D., Lioumis, P., Ilmoniemi, R. J., & Nikulin, V. V. (2008). Bilateral changes in excitability of sensorimotor cortices during unilateral movement: Combined electroencephalographic and transcranial magnetic stimulation study. *Neuroscience*, *152*(4), 1119–1129. https://doi.org/10.1016/j.neuroscience.2008.01.043

Kilavik, B. E., Zaepffel, M., Brovelli, A., MacKay, W. A., & Riehle, A. (2013). The ups and downs of beta oscillations in sensorimotor cortex. *Special Issue: Neuronal Oscillations in Movement Disorders*, *245*, 15–26. https://doi.org/10.1016/j.expneurol.2012.09.014

Kozyrev, V., Eysel, U. T., & Jancke, D. (2014). Voltage-sensitive dye imaging of transcranial magnetic stimulation-induced intracortical dynamics. *Proceedings of the National Academy of Sciences of the United States of America*, *111*(37), 13553–13558. https://doi.org/10.1073/pnas.1405508111

Kruglikov, S. Y., & Schiff, S. J. (2003). Interplay of Electroencephalogram Phase and Auditory-Evoked Neural Activity. *The Journal of Neuroscience*, *23*(31), 10122–10127. https://doi.org/10.1523/JNEUROSCI.23-31-10122.2003

Lefaucheur, J.-P., Aleman, A., Baeken, C., Benninger, D. H., Brunelin, J., Di Lazzaro, V., Filipović, S. R., Grefkes, C., Hasan, A., Hummel, F. C., Jääskeläinen, S. K., Langguth, B., Leocani, L., Londero, A., Nardone, R., Nguyen, J.-P., Nyffeler, T., Oliveira-Maia, A. J., Oliviero, A., … Ziemann, U. (2020). Evidence-based guidelines on the therapeutic use of repetitive transcranial magnetic stimulation (rTMS): An update (2014–2018). *Clinical Neurophysiology*, *131*(2), 474–528. https://doi.org/10.1016/j.clinph.2019.11.002

Lewis, K. J. S., Lewis, C., Roberts, A., Richards, N. A., Evison, C., Pearce, H. A., Lloyd, K., Meudell, A., Edwards, B. M., Robinson, C. A., Poole, R., John, A., Bisson, J. I., & Jones, I. (2022). The effect of the COVID-19 pandemic on mental health in individuals with pre-existing mental illness. *BJPsych Open*, *8*(2), e59. Cambridge Core. https://doi.org/10.1192/bjo.2022.25

Lioumis, P., Kičić, D., Savolainen, P., Mäkelä, J. P., & Kähkönen, S. (2009). Reproducibility of TMS - Evoked EEG responses. *Human Brain Mapping*, *30*(4), 1387–1396. https://doi.org/10.1002/hbm.20608

Litvak, V., Komssi, S., Scherg, M., Hoechstetter, K., Classen, J., Zaaroor, M., Pratt, H., & Kahkonen, S. (2007). Artifact correction and source analysis of early electroencephalographic responses evoked by transcranial magnetic stimulation over primary motor cortex. *NeuroImage*, *37*(1), 56–70. https://doi.org/10.1016/j.neuroimage.2007.05.015

Logothetis, N. K., Guggenberger, H., Peled, S., & Pauls, J. (1999). Functional imaging of the monkey brain. *Nature Neuroscience*, *2*(6), 555–562. https://doi.org/10.1038/9210

Lovinger, D. M. (2008). Communication networks in the brain: Neurons, receptors, neurotransmitters, and alcohol. *Alcohol Research & Health : The Journal of the National Institute on Alcohol Abuse and Alcoholism*, *31*(3), 196–214.

Lusicic, A., Schruers, K. R., Pallanti, S., & Castle, D. J. (2018). Transcranial magnetic stimulation in the treatment of obsessive-compulsive disorder: Current perspectives. *Neuropsychiatric Disease and Treatment*, *14*, 1721–1736. https://doi.org/10.2147/NDT.S121140

Madsen, K. H., Karabanov, A. N., Krohne, L. G., Safeldt, M. G., Tomasevic, L., & Siebner, H. R. (2019). No trace of phase: Corticomotor excitability is not tuned by phase of pericentral mu-rhythm. *Brain Stimulation*, *12*(5), 1261–1270. https://doi.org/10.1016/j.brs.2019.05.005

Mäki, H., & Ilmoniemi, R. J. (2010). The relationship between peripheral and early cortical activation induced by transcranial magnetic stimulation. *Neuroscience Letters*, *478*(1), 24–28. https://doi.org/10.1016/j.neulet.2010.04.059

Massimini, M., Ferrarelli, F., Huber, R., Esser, S. K., Singh, H., & Tononi, G. (2005). Breakdown of Cortical Effective Connectivity During Sleep. *Science*, *309*(5744), 2228–2232. https://doi.org/10.1126/science.1117256

Mazaheri, A., & Jensen, O. (2006). Posterior α activity is not phase-reset by visual stimuli. *Proceedings of the National Academy of Sciences*, *103*(8), 2948–2952. https://doi.org/10.1073/pnas.0505785103

McConnell, K. A., Nahas, Z., Shastri, A., Lorberbaum, J. P., Kozel, F. A., Bohning, D. E., & George, M. S. (2001). The transcranial magnetic stimulation motor threshold depends on the distance from coil to underlying cortex: A replication in healthy adults comparing two methods of assessing the distance to cortex. *Biological Psychiatry*, *49*(5), 454–459. https://doi.org/10.1016/S0006-3223(00)01039-8

Miller, K. J., Hermes, D., Honey, C. J., Hebb, A. O., Ramsey, N. F., Knight, R. T., Ojemann, J. G., & Fetz, E. E. (2012). Human Motor Cortical Activity Is

Selectively Phase-Entrained on Underlying Rhythms. *PLOS Computational Biology*, *8*(9), e1002655. https://doi.org/10.1371/journal.pcbi.1002655

Moliadze, V., Zhao, Y., Eysel, U., & Funke, K. (2003). Effect of transcranial magnetic stimulation on single-unit activity in the cat primary visual cortex. *Journal of Physiology*, *553*(2), 665–679. https://doi.org/10.1113/jphysiol.2003.050153

Mueller, J. K., Grigsby, E. M., Prevosto, V., Petraglia, F. W., Rao, H., Deng, Z.-D., Peterchev, A. V., Sommer, M. A., Egner, T., Platt, M. L., & Grill, W. M. (2014). Simultaneous transcranial magnetic stimulation and single-neuron recording in alert non-human primates. *Nature Neuroscience*, *17*(8), 1130–1136. https://doi.org/10.1038/nn.3751

Nahas, Z., Lomarev, M., Roberts, D. R., Shastri, A., Lorberbaum, J. P., Teneback, C., McConnell, K., Vincent, D. J., Li, X., George, M. S., & Bohning, D. E. (2001). Unilateral left prefrontal transcranial magnetic stimulation (TMS) produces intensity-dependent bilateral effects as measured by interleaved BOLD fMRI. *Biological Psychiatry*, *50*(9), 712–720. https://doi.org/10.1016/S0006-3223(01)01199-4

Nahas, Z., Teneback, C. C., Kozel, A., Speer, A. M., DeBrux, C., Molloy, M., Stallings, L., Spicer, K. M., Arana, G., Bohning, D. E., Risch, S. C., & George, M. S. (2001). Brain Effects of TMS Delivered Over Prefrontal Cortex in Depressed Adults. *The Journal of Neuropsychiatry and Clinical Neurosciences*, *13*(4), 459–470. https://doi.org/10.1176/jnp.13.4.459

Nikulin, V. V., Kičić, D., Kähkönen, S., & Ilmoniemi, R. J. (2003). Modulation of electroencephalographic responses to transcranial magnetic stimulation: Evidence for changes in cortical excitability related to movement. *European Journal of Neuroscience*, *18*(5), 1206–1212. https://doi.org/10.1046/j.1460-9568.2003.02858.x

Nikulin, V. V., Kicic, D., Kahkonen, S., & Ilmoniemi, R. J. (2003). Modulation of electroencephalographic responses to transcranial magnetic stimulation: Evidence for changes in cortical excitability related to movement. *European Journal of Neuroscience*, *18*(5), 1206–1212. https://doi.org/10.1046/j.1460-9568.2003.02858.x

Numssen, O., Zier, A.-L., Thielscher, A., Hartwigsen, G., Knösche, T. R., & Weise, K. (2021). Efficient high-resolution TMS mapping of the human motor cortex by nonlinear regression. *NeuroImage*, *245*, 118654. https://doi.org/10.1016/j.neuroimage.2021.118654

Oathes, D. J., Zimmerman, J. P., Duprat, R., Japp, S. S., Scully, M., Rosenberg, B. M., Flounders, M. W., Long, H., Deluisi, J. A., Elliott, M., Shandler, G., Shinohara, R. T., & Linn, K. A. (2021). Resting fMRI-guided TMS results in subcortical and brain network modulation indexed by interleaved TMS/fMRI. *Experimental Brain Research*, *239*(4), 1165–1178. https://doi.org/10.1007/s00221-021-06036-5

Ohnishi, T., Hayashi, T., Okabe, S., Nonaka, I., Matsuda, H., Iida, H., Imabayashi, E., Watabe, H., Miyake, Y., Ogawa, M., Teramoto, N., Ohta, Y., Ejima, N., Sawada, T., & Ugawa, Y. (2004). Endogenous dopamine release induced by repetitive transcranial magnetic stimulation over the primary motor cortex: An [11C]raclopride positron emission tomography study in anesthetized macaque monkeys. *Biological Psychiatry*, *55*(5), 484–489. https://doi.org/10.1016/j.biopsych.2003.09.016

O'Keeffe, A. B., Malekmohammadi, M., Sparks, H., & Pouratian, N. (2020). Synchrony Drives Motor Cortex Beta Bursting, Waveform Dynamics, and Phase-Amplitude Coupling in Parkinson's Disease. *The Journal of Neuroscience : The Official Journal of the Society for Neuroscience*, *40*(30), 5833–5846. https://doi.org/10.1523/JNEUROSCI.1996-19.2020

Oostenveld, R., Fries, P., Maris, E., & Schoffelen, J. M. (2011a). FieldTrip: Open source software for advanced analysis of MEG, EEG, and invasive electrophysiological data. *Computational Intelligence and Neuroscience*, *2011*. https://doi.org/10.1155/2011/156869

Oostenveld, R., Fries, P., Maris, E., & Schoffelen, J.-M. (2011b). FieldTrip: Open Source Software for Advanced Analysis of MEG, EEG, and Invasive Electrophysiological Data. *Computational Intelligence and Neuroscience*, *2011*, 1–9. https://doi.org/10.1155/2011/156869

Opitz, A., Windhoff, M., Heidemann, R. M., Turner, R., & Thielscher, A. (2011). How the brain tissue shapes the electric field induced by transcranial magnetic stimulation. *NeuroImage*, *58*(3), 849–859. https://doi.org/10.1016/j.neuroimage.2011.06.069

Ozdemir, R. A., Kirkman, S., Magnuson, J. R., Fried, P. J., Pascual-Leone, A., & Shafi, M. M. (2022). Phase matters when there is power: Phasic modulation of corticospinal excitability occurs at high amplitude sensorimotor mu-oscillations. *Neuroimage: Reports*, *2*(4), 100132. https://doi.org/10.1016/j.ynirp.2022.100132

Ozdemir, R. A., Tadayon, E., Boucher, P., Momi, D., Karakhanyan, K. A., Fox, M. D., Halko, M. A., Pascual-Leone, A., Shafi, M. M., & Santarnecchi, E. (2020). Individualized perturbation of the human connectome reveals reproducible biomarkers of network dynamics relevant to cognition.

Proceedings of the National Academy of Sciences, *117*(14), 8115–8125. https://doi.org/10.1073/pnas.1911240117

P. Julkunen. (2019). Mobile Application for Adaptive Threshold Hunting in Transcranial Magnetic Stimulation. *IEEE Transactions on Neural Systems and Rehabilitation Engineering*, *27*(8), 1504–1510. https://doi.org/10.1109/TNSRE.2019.2925904

Paller, K. A., McCarthy, G., Roessler, E., Allison, T., & Wood, C. C. (1992). Potentials evoked in human and monkey medial temporal lobe during auditory and visual oddball paradigms. *Electroencephalography and Clinical Neurophysiology/ Evoked Potentials*, *84*(3), 269–279. https://doi.org/10.1016/0168-5597(92)90008-Y

Paus, T., Sipila, P. K., & Strafella, A. P. (2001). Synchronization of Neuronal Activity in the Human Primary Motor Cortex by Transcranial Magnetic Stimulation: An EEG Study. *Journal of Neurophysiology*, *86*(4), 1983–1990. https://doi.org/10.1152/jn.2001.86.4.1983

Perera, N. D., Alekseichuk, I., Shirinpour, S., Wischnewski, M., Linn, G., Masiello, K., Butler, B., Russ, B. E., Schroeder, C. E., Falchier, A., & Opitz, A. (2023). Dissociation of Centrally and Peripherally Induced Transcranial Magnetic Stimulation Effects in Nonhuman Primates. *The Journal of Neuroscience*, *43*(50), 8649. https://doi.org/10.1523/JNEUROSCI.1016-23.2023

Perera, T., George, M. S., Grammer, G., Janicak, P. G., Pascual-Leone, A., & Wirecki, T. S. (2016). The Clinical TMS Society Consensus Review and Treatment Recommendations for TMS Therapy for Major Depressive Disorder. *Brain Stimulation*, *9*(3), 336–346. https://doi.org/10.1016/j.brs.2016.03.010

Peterchev, A. V., Wagner, T. A., Miranda, P. C., Nitsche, M. A., Paulus, W., Lisanby, S. H., Pascual-Leone, A., & Bikson, M. (2012). Fundamentals of transcranial electric and magnetic stimulation dose: Definition, selection, and reporting practices. *Brain Stimulation*, *5*(4), 435–453. https://doi.org/10.1016/j.brs.2011.10.001

Peters, J. C., Reithler, J., Graaf, T. A. de, Schuhmann, T., Goebel, R., & Sack, A. T. (2020). Concurrent human TMS-EEG-fMRI enables monitoring of oscillatory brain state-dependent gating of cortico-subcortical network activity. *Communications Biology*, *3*(1), 40. https://doi.org/10.1038/s42003-020-0764-0

Petrichella, S., Johnson, N., & He, B. (2017). The influence of corticospinal activity on TMS-evoked activity and connectivity in healthy subjects: A TMS-EEG study. *PLOS ONE*, *12*(4), e0174879. https://doi.org/10.1371/journal.pone.0174879

Premoli, I., Castellanos, N., Rivolta, D., Belardinelli, P., Bajo, R., Zipser, C., Espenhahn, S., Heidegger, T., Müller-Dahlhaus, F., & Ziemann, U. (2014). TMS-EEG Signatures of GABAergic Neurotransmission in the Human Cortex. *Journal of Neuroscience*, *34*(16), 5603–5612. https://doi.org/10.1523/JNEUROSCI.5089-13.2014

Rocchi, L., Di Santo, A., Brown, K., Ibáñez, J., Casula, E., Rawji, V., Di Lazzaro, V., Koch, G., & Rothwell, J. (2021). Disentangling EEG responses to TMS due to cortical and peripheral activations. *Brain Stimulation*, *14*(1), 4–18. https://doi.org/10.1016/j.brs.2020.10.011

Rogasch, N. C., Biabani, M., & Mutanen, T. P. (2022). Designing and comparing cleaning pipelines for TMS-EEG data: A theoretical overview and practical example. *Journal of Neuroscience Methods*, *371*, 109494. https://doi.org/10.1016/j.jneumeth.2022.109494

Rogasch, N. C., Daskalakis, Z. J., & Fitzgerald, P. B. (2013). Mechanisms underlying long-interval cortical inhibition in the human motor cortex: A TMS-EEG study. *Journal of Neurophysiology*, *109*(1), 89–98. https://doi.org/10.1152/jn.00762.2012

Rogasch, N. C., Daskalakis, Z. J., & Fitzgerald, P. B. (2015). Cortical inhibition of distinct mechanisms in the dorsolateral prefrontal cortex is related to working memory performance: A TMS–EEG study. *Cortex*, *64*, 68–77. https://doi.org/10.1016/j.cortex.2014.10.003

Rogasch, N. C., & Fitzgerald, P. B. (2013a). Assessing cortical network properties using TMS-EEG. *Human Brain Mapping*, *34*(7), 1652–1669. https://doi.org/10.1002/hbm.22016

Rogasch, N. C., & Fitzgerald, P. B. (2013b). Assessing cortical network properties using TMS-EEG. *Human Brain Mapping*, *34*(7), 1652–1669. https://doi.org/10.1002/hbm.22016

Romero, M. C., Davare, M., Armendariz, M., & Janssen, P. (2019). Neural effects of transcranial magnetic stimulation at the single-cell level. *Nature Communications*, *10*(1), 1–11. https://doi.org/10.1038/s41467-019-10638-7

Roos, D., Biermann, L., Jarczok, T. A., & Bender, S. (2021). Local Differences in Cortical Excitability – A Systematic Mapping Study of the TMS-Evoked N100 Component. *Frontiers in Neuroscience*, *15*. https://doi.org/10.3389/fnins.2021.623692

Rothwell, J., Hallett, M., Berardelli, A., Eisen, A., Rossini, P., & Paulus, W. (1999). Magnetic stimulation: Motor evoked potentials. The International Federation of Clinical Neurophysiology. *Electroencephalography and Clinical Neurophysiology. Supplement*, *52*, 97—103.

Russo, S., Sarasso, S., Puglisi, G. E., Dal Palù, D., Pigorini, A., Casarotto, S., D'Ambrosio, S., Astolfi, A., Massimini, M., Rosanova, M., & Fecchio, M. (2022). TAAC - TMS Adaptable Auditory Control: A universal tool to mask TMS clicks. *Journal of Neuroscience Methods*, *370*, 109491. https://doi.org/10.1016/j.jneumeth.2022.109491

Saleem, K., & Logothetis, N. (2012). *A combined MRI and histology atlas of the rhesus monkey brain in stereotaxic coordinates* (2nd ed.).

Salvador, R., Silva, S., Basser, P. J., & Miranda, P. C. (2011). Determining which mechanisms lead to activation in the motor cortex: A modeling study of transcranial magnetic stimulation using realistic stimulus waveforms and sulcal geometry. *Clinical Neurophysiology*, *122*(4), 748–758. https://doi.org/10.1016/j.clinph.2010.09.022

Sandbrink, F. (2008). 237 The MEP in clinical neurodiagnosis. In *Oxford Handbook of Transcranial Stimulation*. Oxford University Press. https://doi.org/10.1093/oxfordhb/9780198568926.013.0019

Sarasso, S., Boly, M., Napolitani, M., Gosseries, O., Charland-Verville, V., Casarotto, S., Rosanova, M., Casali, A. G., Brichant, J. F., Boveroux, P., Rex, S., Tononi, G., Laureys, S., & Massimini, M. (2015). Consciousness and complexity during unresponsiveness induced by propofol, xenon, and ketamine. *Current Biology*, *25*(23), 3099–3105. https://doi.org/10.1016/j.cub.2015.10.014

Shirinpour, S., Alekseichuk, I., Mantell, K., & Opitz, A. (2020). Experimental evaluation of methods for real-time EEG phase-specific transcranial magnetic stimulation. *Journal of Neural Engineering*, *17*(4), 046002. https://doi.org/10.1088/1741-2552/ab9dba

Sparks, D. L., Corssen, G., Aizenman, B., & Black, J. (1975). Further studies of the neural mechanisms of ketamine induced anesthesia in the rhesus monkey. *Anesthesia and Analgesia*, *54*(2), 189–195. https://doi.org/10.1213/00000539-197503000-00006

Stokes, M. G., Chambers, C. D., Gould, I. C., English, T., McNaught, E., McDonald, O., & Mattingley, J. B. (2007). Distance-adjusted motor threshold for transcranial magnetic stimulation. *Clinical Neurophysiology*, *118*(7), 1617–1625. https://doi.org/10.1016/j.clinph.2007.04.004

Swann, N. C., Cai, W., Conner, C. R., Pieters, T. A., Claffey, M. P., George, J. S., Aron, A. R., & Tandon, N. (2012). Roles for the pre-supplementary motor area and the right inferior frontal gyrus in stopping action: Electrophysiological responses and functional and structural connectivity. *NeuroImage*, *59*(3), 2860–2870. https://doi.org/10.1016/j.neuroimage.2011.09.049

Thielscher, A., Antunes, A., & Saturnino, G. B. (2015). Field modeling for transcranial magnetic stimulation: A useful tool to understand the physiological effects of TMS? *Proceedings of the Annual International Conference of the IEEE Engineering in Medicine and Biology Society, EMBS*, *2015-Novem*, 222–225. https://doi.org/10.1109/EMBC.2015.7318340

Thielscher, A., Opitz, A., & Windhoff, M. (2011). Impact of the gyral geometry on the electric field induced by transcranial magnetic stimulation. *NeuroImage*, *54*(1), 234–243. https://doi.org/10.1016/j.neuroimage.2010.07.061

Thut, G., Veniero, D., Romei, V., Miniussi, C., Schyns, P., & Gross, J. (2011). Rhythmic TMS Causes Local Entrainment of Natural Oscillatory Signatures. *Current Biology*, *21*(14), 1176–1185. https://doi.org/10.1016/j.cub.2011.05.049

Tononi, G., Sporns, O., & Edelman, G. M. (1994). A measure for brain complexity: Relating functional segregation and integration in the nervous system. *Proceedings of the National Academy of Sciences of the United States of America*, *91*(11), 5033–5037. https://doi.org/10.1073/pnas.91.11.5033

Wagner, J., Wessel, J. R., Ghahremani, A., & Aron, A. R. (2018). Establishing a Right Frontal Beta Signature for Stopping Action in Scalp EEG: Implications for Testing Inhibitory Control in Other Task Contexts. *Journal of Cognitive Neuroscience*, *30*(1), 107–118. https://doi.org/10.1162/jocn_a_01183

Weise, K., Numssen, O., Thielscher, A., Hartwigsen, G., & Knösche, T. R. (2020). A novel approach to localize cortical TMS effects. *NeuroImage*, *209*(March 2019). https://doi.org/10.1016/j.neuroimage.2019.116486

Wischnewski, M., Haigh, Z. J., Shirinpour, S., Alekseichuk, I., & Opitz, A. (2022). The phase of sensorimotor mu and beta oscillations has the opposite effect on corticospinal excitability. *Brain Stimulation*, *15*(5), 1093–1100. https://doi.org/10.1016/j.brs.2022.08.005

Young, K. S., Purves, K. L., Hübel, C., Davies, M. R., Thompson, K. N., Bristow, S., Krebs, G., Danese, A., Hirsch, C., Parsons, C. E., Vassos, E., Adey, B. N., Bright, S., Hegemann, L., Lee, Y. T., Kalsi, G., Monssen, D., Mundy, J., Peel, A. J., … Breen, G. (2023). Depression, anxiety and PTSD symptoms before and during the COVID-19 pandemic in the UK. *Psychological Medicine*, *53*(12), 5428–5441. Cambridge Core. https://doi.org/10.1017/S0033291722002501

Zangen, A., Moshe, H., Martinez, D., Barnea-Ygael, N., Vapnik, T., Bystritsky, A., Duffy, W., Toder, D., Casuto, L., Grosz, M. L., Nunes, E. V., Ward, H., Tendler, A., Feifel, D., Morales, O., Roth, Y., Iosifescu, D. V., Winston, J., Wirecki, T., … George, M. S. (2021). Repetitive transcranial magnetic stimulation for smoking cessation: A pivotal multicenter double-blind randomized controlled trial. *World Psychiatry : Official Journal of the World Psychiatric Association (WPA)*, *20*(3), 397–404. https://doi.org/10.1002/wps.20905

Zazio, A., Miniussi, C., & Bortoletto, M. (2021). Alpha-band cortico-cortical phase synchronization is associated with effective connectivity in the motor network. *Clinical Neurophysiology*, *132*(10), 2473–2480. https://doi.org/10.1016/j.clinph.2021.06.025

Ziemann, U. (2017). Thirty years of transcranial magnetic stimulation: Where do we stand? *Experimental Brain Research*, *235*(4), 973–984. https://doi.org/10.1007/s00221-016-4865-4

Zrenner, C., Desideri, D., Belardinelli, P., & Ziemann, U. (2018). Real-time EEG-defined excitability states determine efficacy of TMS-induced plasticity in human motor cortex. *Brain Stimulation*, *11*(2), 374–389. https://doi.org/10.1016/j.brs.2017.11.016

Appendix

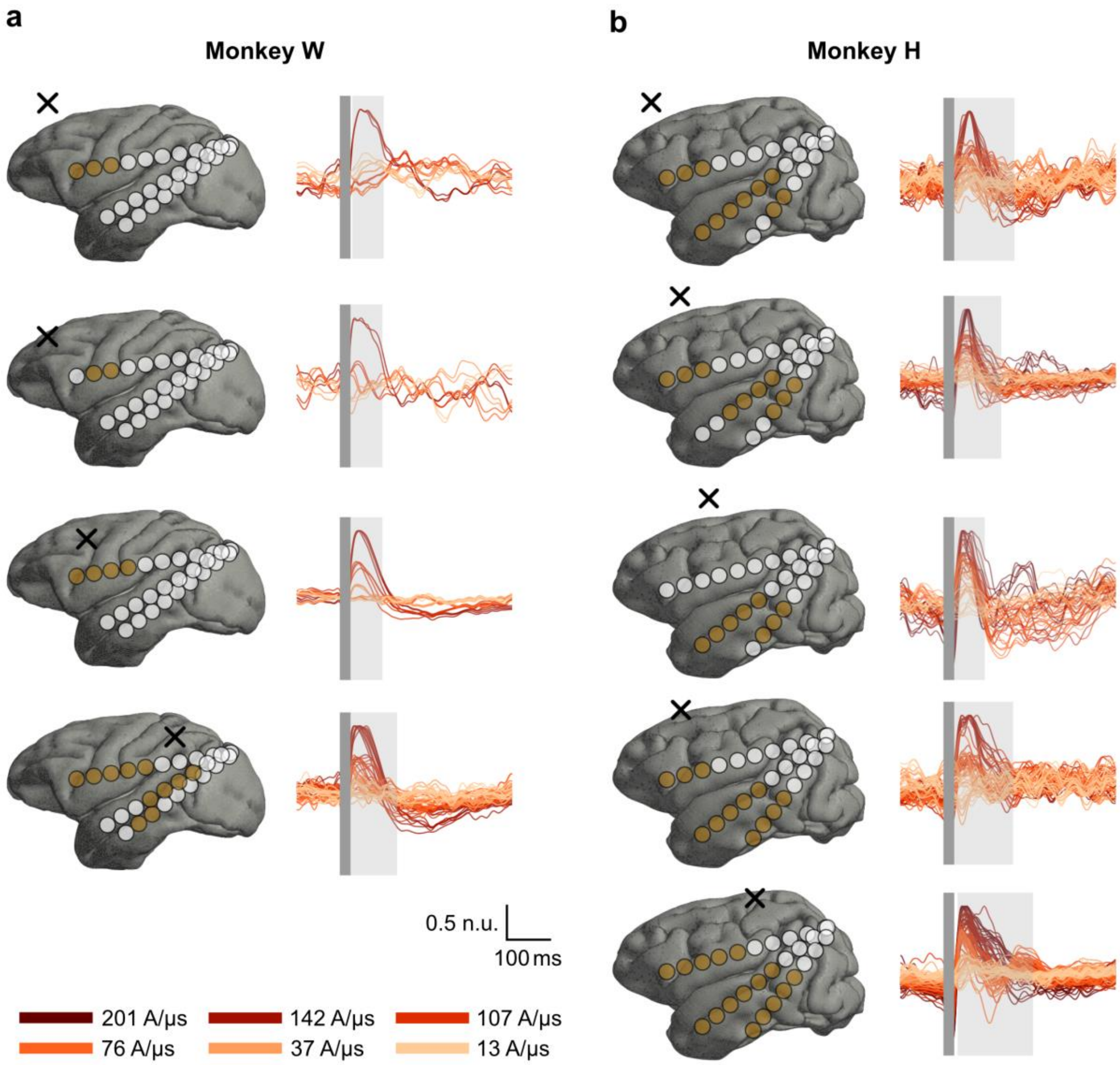

Figure A.1 Local field potentials (LFPs) for each stimulation location. a) Time-locked averaged signal from responsive contacts for each main stimulation location (1-4) in Monkey W. b) Time-locked averaged signals from responsive contacts for each main stimulation location (1-5) in monkey H. All the signals are normalized to the maximum amplitude of each contact. The responsive contacts are shaded in orange on the 3D rendering of the brain. The time window during which a significant effect of stimulation intensity on the LFPs is observed, is shaded in gray for each stimulation location.

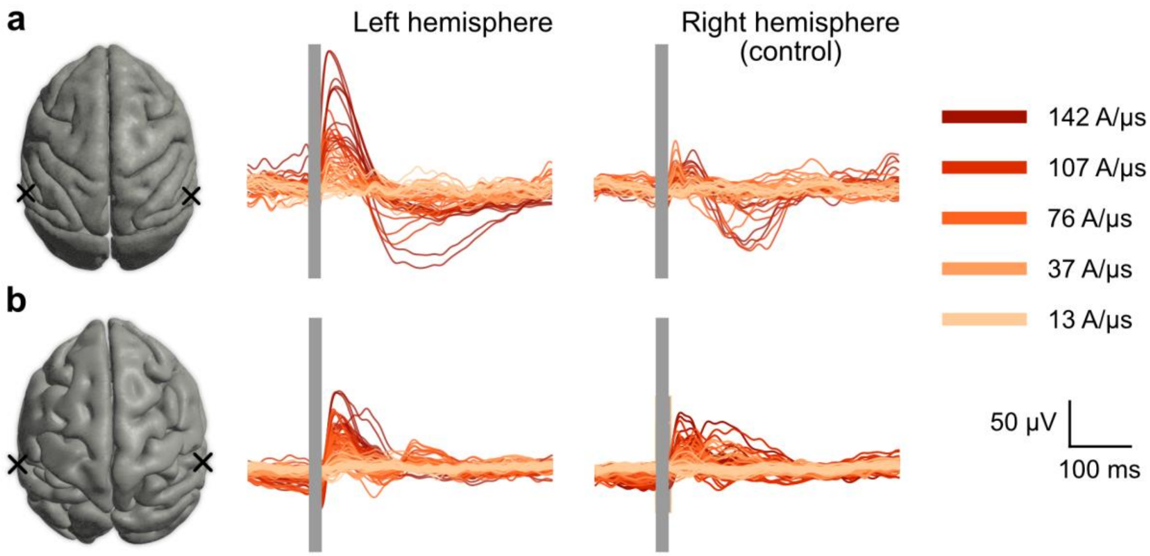

Figure A.2 Comparison of local field potentials between left and right hemispheres. a) The butterfly plot of the local field potentials from all channels when stimulating location 4 (ipsilateral to recording hemisphere) and location 5 (contralateral control location) in Monkey W. In Monkey W, the overall activity is lower when stimulating the control location compared to stimulation location 4. b) Same plots for Monkey H (location 5 – ipsilateral to recording hemisphere and location 6 – contralateral control location). In Monkey H, the control location induces activity in the recording hemisphere albeit less than that of location 5.

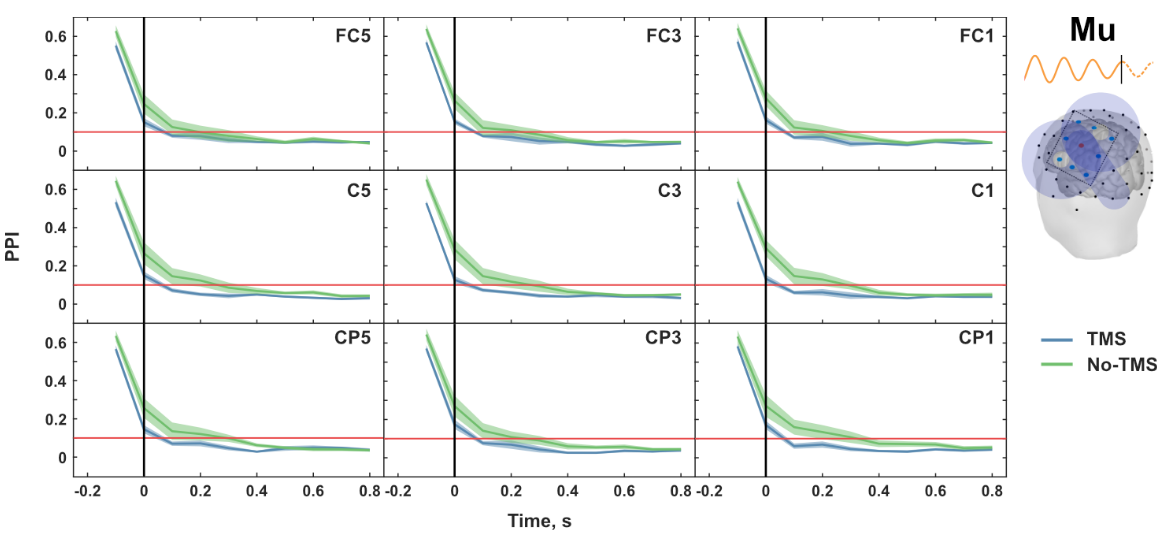

Figure A.3 Phase Preservation Index (PPI) for mu-specific targeting. PPI values are calculated with reference to mu phase at 100 ms prior to TMS pulse, at 100 ms intervals. Blue trace indicates the PPI values for real TMS, and green trace indicates PPI for TMS trigger without actual pulse. Shaded region depicts the standard error of mean (SEM) of PPI. Plots for all electrodes in the Laplacian montage (FC5, FC3, FC1, C5, C3, C1, CP5, CP3 and CP1) are shown here. Black vertical line indicates the TMS trigger, and the red horizontal line (PPI = 0.1) indicates the threshold for phase preservation calculated according to Fischer, 1993. For real TMS condition, there is no substantial evidence for mu phase preservation after TMS delivery.

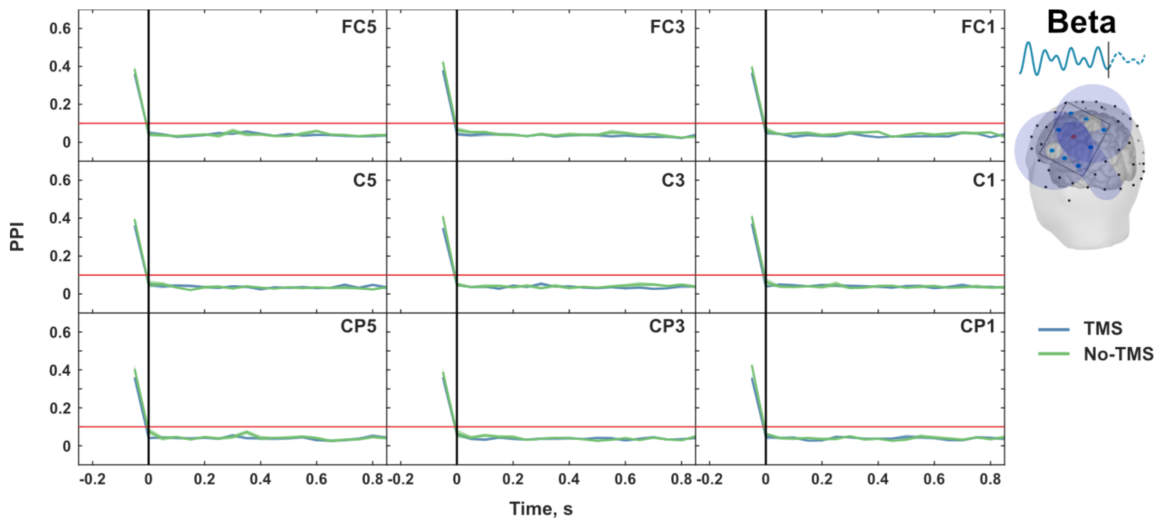

Figure A.4 Phase Preservation Index (PPI) for beta-specific targeting. PPI values are calculated with reference to beta phase at 100 ms prior to TMS pulse, at 100 ms intervals. Blue trace indicates the PPI values for real TMS, and green trace indicates PPI for TMS trigger without actual pulse. Shaded region depicts the standard error of mean (SEM) of PPI. Plots for all electrodes in the Laplacian montage (FC5, FC3, FC1, C5, C3, C1, CP5, CP3 and CP1) are shown here. Black vertical line indicates the TMS trigger, and the red horizontal line (PPI = 0.1) indicates the threshold for phase preservation calculated according to Fischer, 1993. For real TMS condition, there is no substantial evidence for beta phase preservation after TMS delivery.